Human Organ Chips Reveal New Inflammatory Bowel Disease Drivers

Alican Özkan[1], Gwenn E. Merry[1], David B. Chou[1,2], Ryan R. Posey[1], Anna Stejskalova[1], Karina Calderon[1], Megan Sperry[1], Joshua Piatok[1], Viktor Horvath[1,10], Lorenzo E. Ferri[3,4], Emanuela Carlotti[5], Stuart A. C. McDonald[5], Douglas J. Winton[6], Rocco Riccardi[7], Liliana Bordeianou[7], Sean Hall[1,11], Girija Goyal[1], Donald E. Ingber[1,8,9,*]

[1] Wyss Institute for Biologically Inspired Engineering at Harvard University, Boston, MA
[2] Department of Pathology, Massachusetts General Hospital, Boston, MA
[3] Thoracic and Upper GI Cancer Research Laboratories, Research Institute of McGill University Health Centre, Montreal, QC, Canada
[4] Department of Experimental Surgery and Department of Surgery, McGill University, Montreal, QC, Canada
[5] Clonal Dynamics in Epithelia Laboratory, Queen Mary University of London, London, United Kingdom
[6] Cancer Research UK Cambridge Institute, Li Ka Shing Centre, Cambridge, United Kingdom
[7] Department of Surgery, Massachusetts General Hospital, Boston, MA
[8] Vascular Biology Program and Department of Surgery, Boston Children's Hospital and Harvard Medical School, Boston, MA
[9] Harvard John A. Paulson School of Engineering and Applied Sciences, Cambridge, MA
[10] Current address: Entact Bio, Watertown, MA
[11] Current address: Iovance Therapeutics, Tampa, FL

*Address correspondence to: Donald E. Ingber, MD, PhD
201 Brookline Ave., Suite 401, Boston MA, 02215, USA
em: don.ingber@wyss.harvard.edu

Keywords: Organ-on-a-chip, Ulcerative Colitis, Crohn's Disease, Carcinogenesis, Epithelial-Stromal Interactions

Abstract

Inflammatory bowel disease (IBD) patients exhibit compromised intestinal barrier function and decreased mucus accumulation, as well as increased inflammation, fibrosis, and cancer risk, with symptoms often being exacerbated in women during pregnancy. Here, we show that these IBD hallmarks can be replicated using human Organ Chips lined by IBD patient-derived colon epithelial cells interfaced with matched fibroblasts cultured under flow. Use of heterotypic tissue recombinants revealed that IBD fibroblasts are the primary drivers of multiple IBD symptoms. Inflammation and fibrosis are accentuated by peristalsis-like motions in IBD Chips and when exposed to pregnancy-associated hormones in female IBD Chips. Carcinogen exposure also increases inflammation, gene mutations, and chromosome duplication in IBD Chips, but not in Healthy Chips. These data enabled by human Organ Chip technology suggest that the intestinal stroma, sex hormones, and peristalsis-associated mechanical deformations play a key role in driving inflammation, fibrosis, and disease progression in male and female IBD patients.

Main

Inflammation of the intestinal mucosa, including enhanced production of inflammatory cytokines and tissue infiltration with immune cells, along with increased barrier permeability, thinning of the protective mucus layer, and fibrosis are central hallmarks of inflammatory bowel diseases (IBD), such as Crohn's disease (CD) and ulcerative colitis (UC). These alterations lead to significant digestive issues and an increased risk of developing colorectal cancer[1]. IBD symptoms also can be more prominent in women[2] and they have to control their symptoms before pregnancy because many of these patients experience exacerbations that increase the risk of preterm birth[3]. Most IBD treatments target immune cells rather than intestinal tissues, and

57 treatment efficacy is variable among patients[4]. However, interactions between epithelia and
58 underlying stroma also may contribute to inflammation as well as cancer progression[5]. For
59 example, the presence of a subset of fibroblasts that recruit immune cells to the intestinal stem
60 cell niche is associated with poor prognosis in patients with colorectal cancer[6]. Inflamed
61 epithelial cells also can undergo an epithelial-to-mesenchymal transition and increase
62 deposition of extracellular matrix (ECM) resulting in intestinal fibrosis that leads to
63 complications, such as bowel stiffening and restriction of lumenal fluid flow, which further
64 exacerbate digestive problems in IBD patients [7,8]. Thus, there is a need to gain greater insight
65 into how epithelial-stromal interactions, peristalsis, and fluid flow influence IBD development in
66 both male and female patients. However, animal IBD models and in vitro studies with human
67 intestinal cell lines lack direct relevance to the human disease[9], and human intestinal organoids
68 cannot be used to address these questions because they lack an epithelial-stromal interface,
69 mucosal barrier, fluid flow, peristalsis motions, and immune cells, which are critical organ-level
70 features required to address these questions.

71 Here, we leveraged human organ-on-a-chip (Organ Chip) microfluidic culture technology
72 that recreates tissue-tissue interfaces and a physiologically relevant intestinal microenvironment
73 including dynamic fluid flow, peristalsis-like mechanical deformations, and circulating immune
74 cells to confront this challenge[10,11]. Colon Chips lined by human organoid-derived colonic
75 epithelium cultured under dynamic fluid flow have been successfully used in the past to study
76 mucus layer accumulation and physiology[12,13] as well as to identify microbiome metabolites that
77 influence host response to bacterial infections[14]. In this study, we isolated epithelium and
78 stromal-derived fibroblasts from the same regions of colon from healthy or IBD patients and
79 used them to create Colon Chips that contained an epithelial-fibroblast interface. We also
80 created heterotypic tissue recombinant chips, measured the effects of applying peristalsis-like
81 motions and flowing immune cells through the stromal channel, and studied the effects of

82 female hormones on the IBD state, in addition to modeling cancer progression by exposing the
83 Colon Chips to carcinogens in vitro.
84

85 ## Results

86 ### Establishment of Human Healthy and IBD Colon Chips

87 Patient-specific epithelial organoids and stromal fibroblasts were isolated from surgical
88 resections of the colon of healthy and IBD patients with CD or UC (**Extended Data Fig. 1A** and
89 **Supplementary Information**) and the organoids were expanded in Matrigel cultures while the
90 fibroblasts were cultured on plastic dishes (**Extended Data Fig. 1B**). To build the human Colon
91 Chips, the primary colon epithelial cells and fibroblasts were respectively seeded on the top and
92 bottom surfaces of a porous ECM-coated membrane that separates two parallel channels within
93 a commercially available microfluidic Organ Chip (**Fig. 1A**). The cells were allowed to adhere
94 under static conditions for 1 day before flow was initiated. A continuous epithelial monolayer
95 with undulating crypt-like structures formed by 11 days in Healthy Chips when viewed from
96 above (**Fig. 1B,C)** or in cross sections (**Fig. 1D,E**). The epithelium became progressively
97 obscured by dense opaque deposits from day 3 to 7, which completely filled the upper channel
98 by day 11 (**Fig. 1C**). These opaque materials have been shown to be composed of mucus with
99 similar composition, thickness, and bilayer structure as seen in human colonic mucus in vivo
100 [12,13]. Similar chips lined with colonic epithelium and fibroblasts from CD or UC patient samples
101 also formed hill and crypt-like structures, but significantly less mucus accumulated on top of the
102 epithelium, particularly in the UC chips (**Fig. 1C** and **Extended Data Fig. 1C**). Analysis of
103 vertical cross-sectional views of the intestinal epithelium cultured in chips revealed that the
104 heights of the undulating epithelial layerwere significantly reduced in the IBD chips as well (**Fig.
105 1D and Extended Data Fig. 1D**). Epithelial cells within both Healthy and IBD Chips also
106 expressed colon-specific cytokeratin 20 along their apical borders, while the basal stem cell

107 marker SOX9 primarily appeared in their nuclei at the cell base (**Fig. 1F**), which is a hallmark of
108 colon crypts in vivo [15].

109 Past work has shown that there is a subset of stromal fibroblasts in IBD patients that
110 have higher levels of expression of oncostatin M receptor (OSMR) and podoplanin (PDPN)[6],
111 which appear to play a significant role in inflammation, fibrosis, and cancer[16]. Indeed, when we
112 carried out flow cytometric analysis after removing stromal cells from the chips, we found that
113 PDPN expression was significantly higher in IBD fibroblasts that expressed high OSMR levels
114 (**Extended Data Fig. 2A,B**) and that fibroblasts in IBD Chips lined by cells from both CD and
115 UC patients secreted more inflammatory cytokines (e.g, IL6, IL8, MCP-1) from the basal
116 channel than those in Healthy Chips (**Fig. 1G**). We also found that fibroblasts in IBD Chips
117 established using both CD and UC patients samples express higher vimentin and α-SMA than
118 healthy controls (**Extended Data Fig. 2C,D**), as previously observed in IBD mice models
119 induced by treatment with DSS or IL10 knock out[17].

120 Transcriptomic analysis of epithelial cells and fibroblasts individually within Healthy
121 versus IBD Chips revealed that genes which were found to be overexpressed in CD and UC
122 (e.g., ADA2, APOBEC3B, GSPT2, CD40, ACAN, HLA-DQB1) epithelium on-chip were also
123 expressed at higher levels in the intestinal epithelium of IBD patients[18–22] compared to healthy
124 patients (**Extended Data Fig. 3A,B**). In addition, genes suppressed in IBD patient tissues in
125 vivo (e.g., MUC5B, FDFT1 in CD and SOD3, SMIM32, APOBR in UC [18–22]) were expressed at
126 lower levels by epithelium in both CD and UC IBD Chips.

127 When stromal cells cultured in IBD Chips were similarly analyzed, they displayed
128 expression of IBD-relevant genes with CD fibroblasts overexpressing ITGA7, FXD1, HGF,
129 FZD7, NKX2-3, LOXL3 relative to healthy fibroblasts, while high levels of IKBIP, NKX2-3, ADA2,
130 ECM2, NDN, SLC22A17 were seen in UC fibroblasts **(Extended Data. Fig. 3C,D**). In contrast,
131 other genes were downregulated in these fibroblasts including NLRP2, FUCA1, CLCA4, and
132 RNF186 in CD and RALGPS1, DLG3, STON2, and FMO5 in UC derived IBD Chips (**Extended**

133 **Data Fig. 3C,D**), which is again consistent with results of transcriptomic analyses carried out on
134 IBD patient tissues[23–25].
135 Gene ontology and Reactome analysis revealed that multiple IBD-relevant biological
136 processes, including increased ECM production and remodeling, cell adhesion, and
137 angiogenesis as well as decreased metabolism were predominant in both CD and UC
138 epithelium and fibroblasts on-chip, with UC tissues also exhibiting suppressed IL10 signaling
139 (**Extended Data Fig. 4A-D**). These functional pathways are also activated or suppressed in a
140 similar manner in IBD patients[26].

141 **Peristalsis-Like Mechanical Motions Enhance IBD Progression**

142 IBD patients experience thinning of the protective mucus layer in their colon[12] and
143 eventually loss of peristalsis as a consequence of increased fibrosis[7,8], which further exacerbate
144 their gastrointestinal symptoms. However, it is not known whether cyclic mechanical
145 deformation of inflamed intestine or fluid flow due to peristalsis could influence IBD disease
146 progression. To explore this possibility, we cultured Healthy and IBD Chips in the presence or
147 absence of physiologically relevant cyclic deformations by applying suction to side chambers in
148 the flexible devices. The healthy and IBD epithelia both accumulated a mucus layer when
149 exposed to cyclic mechanical deformations were viewed by dark field imaging; however, the
150 layer was much thinner in the IBD Chips (**Fig. 2A,B**). Transcriptomic analysis confirmed that the
151 IBD Chips expressed lower levels of most mucins than Healthy Chips under all conditions, and
152 that while expression of MUC-1,4,12,13,17,3A,5AC, and 5B increased in Healthy Chips
153 exposed to mechanical strain, only MUC5AC and MUC13 increased in the IBD Chips (**Fig. 2C)**.
154 These data show that peristalsis-like mechanical deformations have a direct effect on mucus
155 production in the colonic epithelium in both healthy and IBD Chips as fluid flow was constant
156 under all conditions, and that the IBD epithelium is less effective at maintaining the normal
157 thickness of the mucus layer in vitro as observed in IBD patients in vivo[12,13].

158 Interestingly, second harmonic imaging of ECM fiber formation on-chip revealed that
159 while both CD and UC derived IBD fibroblasts accumulate comparable fibrillar collagen as
160 healthy cells, these levels increase many fold when the IBD Chips are exposed to peristalsis-
161 like motions whereas there is no change in Healthy Chips (**Fig. 2D,E**). Atomic force
162 microscopic analysis carried out in parallel samples from the resections we used to isolate the
163 patient-derived cells confirmed that this was associated with tissue stiffening (**Extended Data**
164 **Fig. 5A-D**). But while transcriptomic analysis showed that there is increased expression of
165 collagen-associated genes in CD and UC stroma on-chip without mechanical strain, exposure to
166 peristalsis-like deformations did not result in significant changes in collagen gene expression
167 (**Fig. 2F**), suggesting that the fibrotic changes we observed resulted from post-transcriptional
168 alterations. Indeed, pathway analysis confirmed that biological processes associated with
169 fibrosis per se (ECM organization, collagen formation and fibril organization) were upregulated
170 in IBD Chips upon exposure to cyclic mechanical deformations (**Extended Fig. 6A**). In addition,
171 our transcriptomic analysis revealed that expression of different cytochrome P450 subunits was
172 suppressed in IBD versus Healthy Chips, which is consistent with the observation that the
173 intestinal tissues of IBD patients experience decreased metabolic activities[27,28]. Importantly,
174 while peristalsis-like cyclic deformations increased the expression of most of these metabolic
175 genes in Healthy Chips, this response was not observed in IBD Chips (**Extended Data Fig. 6B**).
176 Peristalsis-like cyclic deformations also increased barrier permeability in both Healthy
177 and IBD Chips; however, barrier leakiness always remained higher in IBD Chips (**Extended**
178 **Data Fig. 7A**). Mechanical stimulation also enriched expression of inflammation associated
179 genes in epithelial cells and fibroblasts in both Healthy and IBD Chips (**Fig. 2G**) and this was
180 supported by transcriptomic analysis, which showed activation of the inflammatory response
181 pathway in these cells (**Extended Data Fig. 7B**). Importantly, further pathway analysis of this
182 transcriptomic dataset (**Extended Data Fig. 8**) demonstrated that peristalsis-like deformations
183 activate pathways associated with IBD progression and exacerbation in the epithelium, including

184 those involved in cancer, Toll-like receptor signaling, PPAR signaling, and focal adhesion in IBD
185 epithelium (**Extended Data Fig. 9A**) as well as NOD-like receptor signaling, PDGF signaling,
186 and cytokine-cytokine receptor interaction in IBD fibroblasts (**Extended Data Fig. 9B**). In
187 contrast, these pathways that are known to exacerbate colitis in IBD patients[29,30] were not
188 activated in Healthy Chips under the same mechanical stimulation conditions.

189 **Replicating Sex-Specific Clinical Symptoms of IBD Patients**

190 The gastrointestinal symptoms of female IBD patients become much more prominent
191 during menstrual periods[2] and their therapies need to be optimized to control their symptoms
192 before pregnancy due to increased risk of miscarriage, preterm birth and low birthweight[3]. Yet, it
193 is not known whether these responses are a direct effect of ovarian hormones on the intestine,
194 which could potentially contribute to the clinical observations observed in patients [31]. To address
195 this question directly, we exposed healthy and IBD Chips lined by cells from female patients to
196 estrogen (E2) and medroxyprogesterone acetate (MPA) to recapitulate the menstrual cycle or a
197 mixture of pregnancy-associated hormones (E2, MPA, human chorionic gonadotropin, prolactin,
198 and placental lactogen) to mimic the first trimester of pregnancy. Interestingly, exposure to E2
199 and MPA or the pregnancy-associated hormone mixture, increased the height of crypt-like
200 epithelial structures both in healthy and IBD chips (**Fig. 3A-C**). We also discovered addition of
201 E2 and MPA increased fibrosis and exposure to the pregnancy-associated hormone mixture
202 produced an even greater increase in fibrillar collagen deposition in the stroma of IBD Chips;
203 however, this was not observed in Healthy Chips (**Fig. 3D, E and Extended Data. Fig. 10).**
204 Interestingly, exposure to E2, MPA or the pregnancy-associated hormone mixture decreased
205 overall inflammatory cytokine and chemokine production in Healthy Chips whereas levels of
206 these inflammatory molecules increased when IBD Chips were exposed to the same hormones
207 (**Fig. 3F).**

208 **Stromal Fibroblasts Control Barrier Permeability and Epithelial Inflammation**

209 To better understand the role of fibroblasts in IBD, we took advantage of the synthetic
210 biology nature of human Organ Chip technology to create chips lined by heterotypic tissue
211 recombinants of healthy epithelium with IBD stroma and vice versa. As expected, the homotypic
212 cultures of IBD epithelium and stroma had a compromised barrier with higher permeability than
213 healthy epithelium and stroma recombinants (**Fig. 4A**). However, we discovered that the
214 presence of the IBD fibroblasts was the key driver of barrier disruption as permeability increased
215 significantly when they were combined healthy epithelium in tissue recombinant chips, even
216 though there was no difference in permeability when the different epithelia were cultured alone
217 (**Fig. 4A)**. Interestingly, the permeability of the IBD epithelium alone (i.e., without IBD stroma)
218 was similar to that of healthy epithelium with or without healthy fibroblasts, and tissue
219 recombinants combining healthy fibroblasts with IBD epithelium also did not further alter barrier
220 function, again emphasizing the key role of that the IBD stroma plays in terms of compromising
221 intestinal barrier function.
222 This controlling effect of IBD fibroblasts on barrier function when combined with healthy
223 epithelium was also accompanied by increased production of multiple inflammatory cytokines
224 and chemokines including IL-6, MCP-1 (**Fig. 4B**), IL-8, CXCL-1, LIF, IL-21, PIGF-1, and MIP-1b
225 (**Extended Data Fig. 11A**) relative to chips lined by healthy fibroblasts and epithelium or healthy
226 epithelium alone. However, the IBD epithelium appeared to constitutively express high levels of
227 all these cytokines regardless of whether or not IBD fibroblasts were present or they were
228 replaced with healthy fibroblasts, except for production of IL-6 and MCP-1 that were further
229 enhanced by the presence of the IBD stroma (**Fig. 4C** and **Extended Data Fig. 11B**). As these
230 two cytokines are known to promote monocyte infiltration into stroma from the vascular system
231 and their differentiation to macrophages cells[32], we perfused human peripheral blood
232 mononuclear cells (PBMCs) through the basal channel of the Colon Chips. We found that more
233 PBMCs adhered to the stroma and migrated to the epithelial channel in the IBD Chips
234 compared to Healthy Chips (**Fig. 4D**). While application of peristalsis-like deformations did not

235 alter PBMC adhesion to the stroma in the basal channel, it significantly enhanced the migration
236 of these cells to the epithelium in the apical channel, but only in IBD Chips (**Fig. 4E**). However,
237 when we carried out a similar study in a heterotypic tissue recombinant chip containing IBD
238 epithelium with healthy fibroblasts, PBMC recruitment and migration were suppressed and
239 reverted to the low levels observed in Healthy Chips (**Fig. 4D,E**). This finding correlates well
240 with transcriptomic analysis, which revealed that multiple surface receptors for immune cell
241 adhesion are expressed at higher levels in fibroblasts and epithelium in IBD Chips versus
242 Healthy Chips (**Extended Data Fig. 11C**). IBD Chips co-cultured with PBMCs also showed
243 increased production of IL-6 and IL-8 in both their apical and basal channels, whereas this was
244 not observed when Healthy Chips (**Extended Data Fig. 11D**).

245 **Modeling Early Cancer Progression in Human IBD Chips**

246 Patients with IBD have a higher incidence of colorectal cancer formation[33] and this also
247 has been demonstrated in animal IBD models by exposing them to the carcinogen ENU[34].
248 When we exposed Healthy and IBD Chips created with cells from multiple different donors to
249 ENU (10 μg/ml) for 3 weeks, we observed a decrease in the height of crypt-like structures (**Fig.**
250 **5A,B**) and an increase in barrier permeability (**Fig. 5C**) in both in healthy and IBD Chips.
251 However, ENU had a much greater impact on inflammatory cytokine secretion in the IBD Chips
252 (**Fig. 5D**) and it resulted in a greater reduction of E-cadherin expression in IBD Chips versus
253 Healthy Chips, which was accompanied by a concomitant increase in β-catenin translocation to
254 the nucleus (**Fig. 5E,F**). Similar activation of the β-catenin signaling pathway has previously
255 been shown to be associated with colorectal cancer progression[35]. In addition, ENU treatment
256 promoted enlargement of epithelial nuclei and a decrease in their roundness, which are also
257 known to accompany early carcinogenesis[36]. Importantly, shallow pass genome sequencing
258 revealed increased gene mutations and duplication in IBD Chips, but not in Healthy Chips (**Fig.**
259 **5G**). Interestingly, the CD chips exhibited a higher level of gene amplification than chips lined

260 with cells from UC patients, and an existing mutation in one CD patient was further amplified
261 after ENU exposure.

262 We then investigated whether the fibroblast phenotype influences the propensity for
263 cancer formation following ENU exposure in healthy versus IBD epithelium cultured on-chip.
264 CEACAM5 is an early stage colorectal cancer (CRC) marker[37], which is expressed in only CRC
265 tissues and not in healthy and IBD intestinal epithelium in vivo (**Extended Figure 12A**). When
266 we analyzed its expression in epithelium in our heterotypic and homotypic tissue recombinants
267 on-chip, we found that neither healthy nor IBD epithelium expressed CEACAM5 on-chip under
268 baseline conditions without ENU exposure (**Extended Data Fig. 12B).** Importantly, healthy
269 epithelium exposed to ENU expressed CECAM5, but only when cultured with IBD fibroblasts
270 (**Fig. 5H and Extended Data Fig.12C**). The presence of IBD fibroblasts also enhanced
271 expression of CEACAM5 in IBD epithelium when exposed to ENU, although lower levels of
272 CEACAM5 expression were even observed when IBD epithelium was cultured alone or with
273 healthy fibroblasts. A greater reduction in E-cadherin expression (**Extended Data Fig. 12D,E**),
274 along with β-catenin translocation to the nucleus also were seen in IBD epithelium cultured with
275 IBD fibroblasts when exposed to ENU (**Extended Data Fig. 12F**). Taken together, these data
276 show that IBD fibroblasts play a significant role in driving a increased propensity for cancer
277 initiation in intestinal epithelium.

278

279 **Discussion**

280 Taken together, these findings show that human Colon Chips created with primary
281 patient-derived colonic epithelium and fibroblasts from both healthy and IBD patients
282 recapitulate many features of their respective healthy and diseased phenotypes that are
283 observed in vivo. Based on its synthetic nature, this model enabled exploration of the roles of
284 stromal fibroblasts, epithelium, and immune cells, as well as fluid flow and peristalsis-like
285 mechanical deformations in the etiology of this disease. Importantly, our results revealed that

286 the stroma is a key driver of the IBD phenotype as it is appears to drive effects on intestinal
287 permeability, inflammation, and immune cell infiltration in human intestinal tissues. The finding
288 that IBD stromal fibroblasts respond differently to physiological peristalsis motions than healthy
289 fibroblasts and exhibits enhanced inflammation and fibrotic responses while fluid flow was
290 maintained constant also suggests that physiological mechanical deformations of intestine
291 during early stages of IBD development may feed back to further enhance inflammation and
292 fibrosis thereby accelerating disease progression. In addition, we found that ovarian hormones
293 influence the IBD phenotype directly by targeting the intestinal stroma and enhancing
294 inflammation and fibrosis. .

295 Finally, we demonstrated that the human IBD Chips also exhibit an enhanced sensitivity
296 to a carcinogen and undergo changes that underlie early stages of carcinogenesis in vitro,
297 which is again consistent with the finding that IBD patients have an increased propensity to
298 develop colorectal cancers. Our finding that intestinal stromal fibroblasts influence immune cell
299 trafficking is consistent with a past study in which knock out of genes expressed in an
300 inflammatory subset of fibroblasts produced a similar effect in a mice DSS colitis model[12].
301 These results raise the possibility that human Colon Chips could be used as a preclinical model
302 with IBD patient cells to study the effects of emerging immune cell targeting therapies (e.g., anti-
303 integrin $\alpha 4\beta 7$ to suppress infiltration of circulating T-cells) on IBD stroma versus epithelium and
304 to determine their potential efficacy in a patient-specific manner[39]. In addition, this work might
305 serve as inspiration to develop other stroma-targeted therapies given our findings that the
306 stroma is a key driver of the IBD state in both females and males. The stroma also plays a
307 critical role in intestinal homeostasis by supporting the intestinal stem cell niche growth and
308 modulating immune responses, as well as protection against microbiota[40].

309 Another novel feature of this study is its relevance for Women's Health. Female IBD patients
310 can experienced loose and increased stools during the menstrual cycle as well as greater fetal
311 complications during pregnancy [31,41]. However, it has not been possible in the past to explore

312 whether or not these symptoms are the result of direct effects of female hormones on intestinal
313 tissues. This is because female hormone research is challenging using animals. For example,
314 mice that are often used for women's health research[42] do not menstruate like humans do (e.g.,
315 they undergo an estrous cycle) and their immune responses different significantly from human[43].
316 Because biopsy collection during menstruation or pregnancy is not easily done in a clinical
317 setting, it is also challenging to understand the biological basis for clinical symptoms observed
318 in female IBD patients. Another advantage of our model is that we can measure the direct
319 effects of these hormones on healthy versus IBD intestinal tissues. Our finding that pregancy
320 hormones directly enhance inflammation and fibrosis in Colon Chips, particularly in female IBD
321 Chips could be at least in part explain the exacerbation of IBD symptoms symptoms observed
322 during pregnancy in 30-35% of female IBD patients[38]. We also observed an increase in the
323 height of crypt-like structures in Colon Chips as a result of exposure to pregnancy-associated
324 hormones both in healthy and IBD chips. A similar increase in villi height was observed in the
325 small intestine of healthy pregnant mice, and this increased surface area is thought to support
326 increased nutrient absorption for the fetus.[44,45] However, our results showing that the colonic
327 epithelium undergo similar expansion in response to pregnancy hormones in both healthy and
328 IBD tissues suggests that this may not be limited to nutrient absorption, and also include water
329 and electrolyte reabsorption. Thus, these data provide new insights into how female hormones
330 influence intestinal physiology in both healthy and IBD patients.
331 In addition to increased inflammation and decreased mucus production, lack of intestinal
332 motion due to fibrosis is a hallmark of IBD; however, it has not been previously possible to
333 explore whether peristalsis plays a role in earlier stages of IBD progression. We found that
334 peristalsis-like mechanical deformations increased production of the protective mucus layer in
335 Healthy Chips, but less so in IBD Chips, and that these mechanical cues also enhanced
336 inflammation and fibrosis, but only in IBD Chips. This suggests that persistence of physiological
337 peristalsis during early stages of inflammation may promote progression of IBD, and that fibrosis

338 and resultant suppression of peristalsis likely occur at a later stage in this process. This may, in
339 part, occur because the IBD tissues lose their ability to maintain the mucus barrier that protects
340 against dysbiotic microbiome and pathogens that are known to be enriched in the microbiome of
341 IBD patients, such as *Ruminococcus* family members that degrade mucus[46]. This could then
342 lead to more inflammation and a positive feedback loop characterized by enhanced sensitivity to
343 these mechanical deformations resulting in greater increases in inflammation, ECM
344 accumulation, and fibrosis at later stages of the disease, which stiffens the mucosa and
345 physically restricts tissue distension.[41]
346 Chronic inflammation in patients with IBD is known to be a risk factor for increased cancer
347 formation. Importantly, our results show that human IBD tissues do indeed exhibit an enhanced
348 sensitivity to a carcinogen (ENU) compared to Healthy colon tissues on-chip, as indicated by
349 crypt blunting, loss of adherent junctions, overexpression of the early stage CRC marker
350 CEACAM5, and localization of β-catenin to the nucleus as seen in IBD patient tissues that
351 progress to colorectal cancer[47]. Importantly, we also observed a greatly increased inflammatory
352 response as well as accelerated development of cancer-associated mutations and
353 chromosomal amplifications in IBD Chips but not Healthy Chips, even though immune cells
354 were not present. While similar effects have been observed after exposure to ENU in a murine
355 intestine model [48], this to our knowledge is the first demonstration of early cancer progression in
356 a preclinical *human* IBD model. Although it has been believed that both CD and UC patients
357 carry a similarly high risk of cancer progression [49], many CD patients undergo colectomy early
358 in the course of the disease to alleviate persistent symptoms[50], and this effectively eliminates
359 their risk of developing colorectal cancer.[59] Interestingly, although our sampling was small, we
360 found that ENU induced greater gene and chromosomal aberrations in CD patient tissues than
361 in UC patient chips, suggesting that they might exhibit a greater susceptibility to carcinogens.
362 More importantly, use of Organ Chip technology enabled us to create tissue recombinant
363 models, which revealed that IBD fibroblasts play a central role in driving this increased

364 propensity for cancer formation. This result is consistent with finding that cancer-associated
365 fibroblasts also promote a dysplastic transition in metaplastic gastric epithelial cells.[51] This is a
366 finding which should be followed up in clinical studies in the future.

367 The incidence of IBD is anticipated to increase in the upcoming years. Limitations in the
368 ability of in vivo models to represent human IBD physiology are evident, as the most commonly
369 used anti-TNF and anti-IL-12/23p40 antibodies, which benefit patients with IBD, are generally
370 not effective in chemically-induced colitis models[52]. The need for modeling IBD using Organ
371 Chip technology also has been acknowledged by leading IBD organizations, such as the
372 Crohn's and Colitis Foundation[53]. Therefore, we believe this novel microfluidic disease model
373 brings important opportunities for IBD treatment, management, and drug development. As we
374 can analyze outflows from the epithelial and stromal compartments separately and through use
375 of tissue recombinants, this method also may facilitate discovery of potential stool and blood
376 biomarkers of IBD progression and cancer risk as well as response to therapy. Use of tissue
377 recombinants is a powerful method for analyzing epithelial-mesenchymal interactions in
378 commonly used developmental biology research, which as we show here also may be applied
379 to confront similar questions relating to human epithelial-stromal interactions, which are
380 challenging to address in vivo. In addition to enabling study of the effects of female hormones
381 on IBD, and it also could allow investigation of other IBD subcategories, including very early
382 onset (VEO-IBD), adolescent IBD, and genetic forms of the disease by lining chips with relevant
383 patient cells.

384 While this model recapitulates IBD-associated features observed in the human colon,
385 other intestinal regions such as the ileum, duodenum, jejunum, and rectum, could also be
386 modeled using IBD tissues collected from these sites. Modeling these additional regions,
387 particularly the small intestine, would be valuable for investigating absorption and metabolism-
388 related complications in IBD. Notably, Organ Chip technology has already enabled the modeling
389 of these regions using tissues collected from healthy patients[54–56] . Diet can also influence

390 exacerbation of colitis and a small intestine IBD model could be beneficial to investigate diet-
391 associated features in IBD, given that short chain fatty acids (SCFAs), such as butyrate,
392 produced by healthy microbiome can affect IBD remission[57,58]. While we modeled epithelial-
393 stromal interactions in IBD chips, other IBD specific features. such as ileitis-associated fat
394 creeping. can be modeled as well by including adipocytes in the model. In this study, we co-
395 cultured immune cells alongside disease-specific epithelial cells and fibroblasts. This capability
396 can enable evaluation of immune cell-targeting therapeutics, such as α4β7, TL1A, JAK, TNF-α
397 and IL-23 inhibitors[59], alone or when combined with each other for their potential downstream
398 effects on mucosal tissues and associated complications. Particularly fibrosis has been an
399 unmet challenge in management of IBD in patients as well as other fibrotic diseases (e.g. cystic
400 fibrosis, non-alcoholic fatty liver disease, nonalcoholic steatohepatitis and idiopathic pulmonary
401 fibrosis). Finally, given the synthetic nature of the model and as living gut microbiome can be
402 co-cultured in these Intestine Chips for extended times[54,60], this experimental system also may
403 be used to study how other environmental factors (such as pathogens) contribute to
404 development of the IBD phenotype in the future.

405 **Methods**

406 **Acquisition of human colon tissue and cells**

407 Healthy colon tissue samples were collected from macroscopically grossly unaffected
408 regions of the colon of de-identified healthy adult patients undergoing endoscopy for non-IBD
409 related complaints, such as diverticulitis. IBD tissue samples were collected from tissue
410 resections from IBD patients with either CD disease or Ulcerative Colitis. Informed consent and
411 developmentally appropriate assent were obtained at Massachusetts General Hospital and
412 McGill University Health Centre from the donors. All methods were performed in accordance
413 with the Institutional Review Board of Massachusetts General Hospital approval (protocol
414 number IRB-2015P001859) and McGill University Health Centre (protocol number REB-2007-
415 856). We generated epithelium-derived organoids (colonoids) that were cultured in Matrigel

416 using published methods[13,54]and isolated stromal fibroblasts from the same IBD tissues from 3
417 CD and 4 UC patients, which were cultured in fibroblast medium (FM, CC-3132, Lonza, MA) in
418 75 cm^2 flasks (3531135, Falcon, Durham, NC) with Primocin (100 μg/ml) replaing the GA
419 supplement. Healthy colonoids and fibroblasts were isolated from areas with normal histology
420 adjacent to regions of diverticulitis from 4 otherwise healthy patients (**Supplementary Table 1**).
421 The donor cells used across the experiments were provided in **Supplementary Table 2**. All
422 reagents and resources were provided in **Supplementary Table 3**.

423 **Human Colon Chip Cultures**

424 Our methods for creating and culturing human Colon Chips lined by primary intestinal
425 organoid-derived epithelium using commercially available Organ Chip Devices (Basic Research
426 Kit; Emulate Inc.) have been described previously[13,61] and are described in greater detail in
427 Supplementary Materials. Colonoids cultured were released from Matrigel and fragmented by
428 treatment with TrypLE Express Enzyme (12605010; Thermo Fisher Scientific), before being
429 seeded in the apical channel of the 2-channel Organ Chip devices and incubated overnight at
430 37° C under 5% CO_2 to promote adhesion. One day later, channels were washed with
431 Expansion Medium (EM) to remove unattached cells, and then perfused with EM (60 μL/hr). At
432 this time, the cultured fibroblasts were detached enzymatically and seeded in EM in the basal
433 channel for 2 h under static conditions to promote adhesion. After washing, EM was then
434 perfused through both channels at 60 μL/h. After 3 days of co-culture during which both
435 epithelial and fibroblast monolayers were established, EM perfused through the apical channel
436 was changed to Hank's balanced salt solution (HBSS) with calcium and magnesium (21-023-cv;
437 Corning) supplemented with 100 mg/mL Primocin (ant-pm-1; InvivoGen) while EM remained
438 flowing through the basal channel. For experiments exploring the role of physiological
439 peristalsis-like motions, cyclic mechanical strain (10% Strain 0.15 Hz) was applied to the tissues
440 by applying cyclic suction to side chambers of the flexible device[54,61] for 2 weeks after seeding.

441 Methods for morphological analysis, cytokine quantification, flow cytometry, transcriptional
442 analysis, and atomic force microscopy can be found in **Supplementary Information**.
443
444 **Maternal Hormone Treatment**
445 Established Healthy and IBD Colon Chips were exposed to different combinations of
446 hormones from basal channel to recapitulate either the menstrual cycle or first trimester of
447 pregnancy. Chips were treated with 17β-estradiol (E2, 10 nM, Sigma, E4389) for 3 days before
448 being exposed to medroxyprogesterone 17-acetate (MPA, 1 μM, Sigma, 46412-250MG) for an
449 additional 4 days to mimic the menstrual period of the cycle. Chips perfused for 3 days with E2
450 were then treated with E2, MPA, Prolactin (PRL, 20 ng/mL, VWR, 10770-682), Human Placental
451 Lactogen/CSH1 (hPL, 20 ng/ml, R&D, 5757-PL), and Human Chorionic Gonadotropin (HCG, 1
452 μg/mL, VWR, IC0219859110) for 4 days to recapitulate the first trimester of pregnancy as
453 described previously[62,63].
454 **Immune Cell Recruitment Assay**
455 Colon Chips were cultured for 2 weeks before human peripheral blood mononuclear
456 cells (PBMCs) were added to the cultures for studies on immune cell adhesion and migration.
457 PBMCs were collected from anonymous donors undergoing stem cell mobilization at the
458 Massachusetts General Hospital (MGH) under Institutional Review Board approved protocol
459 #2015P001859. PBMCs were freshly isolated by density centrifugation using the Lymphoprep
460 protocol (StemCell Technologies, #07801), resuspended in 10 ml of DMEM containing 10%
461 FBS(10082-147) and 1% Penicillin-Streptomycin (P4333-100ML), and labeled with 10 μl of
462 CellTracker Deep Red at a final concentration of 10 μM (Invitrogen, #C34565) for 20 minutes at
463 37°C. The labeled cells were centrifuged and resuspended to a concentration of 5×10^7 cells/ml
464 and 25 μl of the PBMC suspension was added to the lower channel (see **Supplementary**
465 **Information** for more details).
466 **Analysis of effects of carcinogen exposure**

467 To explore if the chip models can be used to study the effects of intestinal tissue to
468 carcinogen exposure in vitro, Healthy and IBD Colon Chips were exposed to 10 μg/mL of N-
469 ethyl-N-nitrosourea (ENU, Millipore Sigma, N8509), which was flowed through both the apical
470 and basal channels at 60 μL/hr. Chips were harvested for DNA isolation three weeks after ENU
471 exposure. Briefly, chips were washed with DPBS (-/-) and incubated with TrypLE consisting of 2
472 mg/mL collagenase-I (Thermo Fisher Scientific, 17100-017) and 10 μM Y-27632 (Y0503;
473 Sigma-Aldrich, St. Louis, MO) at 37ºC for 1 h. Single cells were washed with DPBS (-/-) and
474 DNA was isolated by following the manufacturer's protocol (Qiagen Micro DNA isolation kit, Cat:
475 56304 Qiagen, Germany). Shallow whole genome sequencing was performed in two batches
476 using different methods (see **Supplementary Information**). The raw sequence reads were
477 mapped to *Homo sapiens* GRCh38 with Burrows-Wheeler Alignment Tool v0.7.17[64]. Reads with
478 a mapping quality of less than 37 were removed from further analysis. The PCR duplicates and
479 base quality recalibration were subsequently carried out using Genome Analysis Toolkit (GATK)
480 v4.4.0[65] and Picard v2.27.5. The copy number of the genome was then estimated and profiled
481 with ACE v3.16[66] and QDNAseq v1.35.0 R package[67] using 100 Mb fixed-sized bins.

482 **Statistical Analysis**

483 Data in all graphs are expressed as mean ± standard deviation (SD) and significant
484 differences between multiple groups were determined using an unpaired Students t-test, one-
485 way analysis of variance (ANOVA) or two-way ANOVA with Tukey test for correction unless
486 otherwise indicated in the figure legends. $P<0.05$ was considered significant. Data were
487 analyzed using GraphPad Prism 8 software (GraphPad Software, San Diego, CA).

488 **Acknowledgement**

489 This work was funded in part by Cancer Research UK (C19767/A27145 to D.E.I.) and by
490 the Wyss Institute for Biologically Inspired Engineering at Harvard University as well as by an
491 NIH training grants (5T32DK007199-44 and 5T32EB016652-10 to A.Ö.) and Wyss Technology

492 Development Fellowship to A.Ö. We thank Harvard Digestive Diseases Center Organoid Core
493 for providing L-WRN conditioned media (P30DK034854).

494 **Contributions**

495 A.O., S.H. and D.E.I designed the research; A.O., G.E.M, R.R.P. A.S. K. C., E. C., J.P.
496 performed the experiments; A.O., G.E.M., R.R.P. A.S., K.C., E.C. analyzed and interpreted the
497 data; A.O. and G.E.M. established healthy and IBD human organoid and fibroblast biobanks; V.
498 H., M. S. and A.O. performed bioinformatic analysis; D.B.C., L.E.F., R.R., L.B. provided the
499 clinical samples; A.O. and D.E.I. acquired the funding; A.O. wrote the articled with input from
500 G.G., S.H. and D.E.I.; and all authors reviewed, discussed and edited the manuscript.

501 **Data and code availability**

502 Data that support the findings of this study are available within the paper and its
503 Supplementary Information files. The RNA sequencing data have been deposited in the Gene
504 Expression Omnibus (GEO) with the accession code GSE277964. All data reported in this study
505 are available in the Source Data files. Any other material including the R code used for data
506 analysis is available upon reasonable request.

507 **Competing interests**

508 D.E.I. holds equity in Emulate, chairs its scientific advisory board and is a member of its board
509 of directors. The other authors declare no competing interests.

510 **References**

511 1. Friedrich, M. *et al.* IL-1-driven stromal–neutrophil interactions define a subset of patients
512 with inflammatory bowel disease that does not respond to therapies. *Nat Med* **27**, 1970–
513 1981 (2021).
514 2. Goodman, W. A., Erkkila, I. P. & Pizarro, T. T. Sex matters: impact on pathogenesis,
515 presentation and treatment of inflammatory bowel disease. *Nature Reviews*
516 *Gastroenterology & Hepatology 2020 17:12* **17**, 740–754 (2020).
517 3. Watermeyer, G. Pregnancy and inflammatory bowel disease. *South African*
518 *Gastroenterology Review* **5**, 4–6 (2007).

519 4. Sarvestani, S. K. *et al.* Cancer-predicting transcriptomic and epigenetic signatures
520 revealed for ulcerative colitis in patient-derived epithelial organoids. *Oncotarget* **9**,
521 28717–28730 (2018).
522 5. Ingber, D. E. Cancer as a disease of epithelial–mesenchymal interactions and
523 extracellular matrix regulation. *Differentiation* **70**, 547–560 (2002).
524 6. Smillie, C. S. *et al.* Intra- and Inter-cellular Rewiring of the Human Colon during Ulcerative
525 Colitis. *Cell* **178**, 714-730.e22 (2019).
526 7. Rieder, F. & Fiocchi, C. Intestinal fibrosis in IBD - A dynamic, multifactorial process. *Nat*
527 *Rev Gastroenterol Hepatol* **6**, 228–235 (2009).
528 8. Guglielmo, F. F. *et al.* Identifying decreased peristalsis of abnormal small bowel
529 segments in Crohn's disease using cine MR enterography: the frozen bowel sign. *Abdom*
530 *Imaging* **40**, 1150–1156 (2015).
531 9. Joshi, A., Soni, A. & Acharya, S. In vitro models and ex vivo systems used in
532 inflammatory bowel disease. *In vitro models 2022 1:3* **1**, 213–227 (2022).
533 10. Özkan, A., LoGrande, N. T., Feitor, J. F., Goyal, G. & Ingber, D. E. Intestinal organ chips
534 for disease modelling and personalized medicine. *Nat Rev Gastroenterol Hepatol* 1–23
535 (2024) doi:10.1038/s41575-024-00968-3.
536 11. Ingber, D. E. Human organs-on-chips for disease modelling, drug development and
537 personalized medicine. *Nat Rev Genet* **23**, 467–491 (2022).
538 12. Gustafsson, J. K. & Johansson, M. E. V. The role of goblet cells and mucus in intestinal
539 homeostasis. *Nat Rev Gastroenterol Hepatol* **19**, 785–803 (2022).
540 13. Sontheimer-Phelps, A. *et al.* Human Colon-on-a-Chip Enables Continuous In Vitro
541 Analysis of Colon Mucus Layer Accumulation and Physiology. *Cmgh* **9**, 507–526 (2020).
542 14. Tovaglieri, A. *et al.* Species-specific enhancement of enterohemorrhagic E. coli
543 pathogenesis mediated by microbiome metabolites. *Microbiome* **7**, 1–21 (2019).
544 15. Chan, C. W. M. *et al.* Gastrointestinal differentiation marker Cytokeratin 20 is regulated
545 by homeobox gene CDX. *Proc Natl Acad Sci U S A* **106**, 1936–1941 (2009).
546 16. West, N. R. *et al.* Oncostatin M drives intestinal inflammation and predicts response to
547 tumor necrosis factor–neutralizing therapy in patients with inflammatory bowel disease.
548 *Nat Med* **23**, 579–589 (2017).
549 17. Wu, J. *et al.* Therapeutic targeting of vimentin by ALD-R491 impacts multiple pathogenic
550 processes to attenuate acute and chronic colitis in mice. *Biomedicine & Pharmacotherapy*
551 **168**, 115648 (2023).

552 18. Torres, J. *et al.* Serum Biomarkers Identify Patients Who Will Develop Inflammatory
553 Bowel Diseases Up to 5 Years Before Diagnosis. *Gastroenterology* **159**, 96–104 (2020).
554 19. Danese, S., Sans, M. & Fiocchi, C. The CD40/CD40L costimulatory pathway in
555 inflammatory bowel disease. *Gut* **53**, 1035 (2004).
556 20. Liu, Z. *et al.* Genetic architecture of the inflammatory bowel diseases across East Asian
557 and European ancestries. *Nat Genet* **55**, 796 (2023).
558 21. Tian, T., Wang, Z. & Zhang, J. Pathomechanisms of Oxidative Stress in Inflammatory
559 Bowel Disease and Potential Antioxidant Therapies. *Oxid Med Cell Longev* **2017**,
560 4535194 (2017).
561 22. Stokkers, P. C. F., Reitsma, P. H., Tytgat, G. N. J. & Van Deventer, S. J. H. HLA-DR and
562 -DQ phenotypes in inflammatory bowel disease: a meta-analysis. *Gut* **45**, 395 (1999).
563 23. Yu, W. *et al.* Association of a Nkx2-3 polymorphism with Crohn's disease and expression
564 of Nkx2-3 is up-regulated in B cell lines and intestinal tissues with Crohn's disease. *J*
565 *Crohns Colitis* **3**, 189–195 (2009).
566 24. WO2019018571A1 - Methods and uses of inflammatory bowel disease biomarkers -
567 Google Patents. https://patents.google.com/patent/WO2019018571A1/en.
568 25. Srivastava, M., Zurakowski, D., Cheifetz, P., Leichtner, A. & Bousvaros, A. Elevated
569 Serum Hepatocyte Growth Factor in Children and Young Adults With Inflammatory Bowel
570 Disease. *J Pediatr Gastroenterol Nutr* **33**, 548–553 (2001).
571 26. Cheng, C. *et al.* Identification of differentially expressed genes, associated functional
572 terms pathways, and candidate diagnostic biomarkers in inflammatory bowel diseases by
573 bioinformatics analysis. *Exp Ther Med* **18**, 278–288 (2019).
574 27. Wilson, A. *et al.* Crohn's Disease Is Associated with Decreased CYP3A4 and P-
575 Glycoprotein Protein Expression. *Mol Pharm* **16**, 4059–4064 (2019).
576 28. Sen, A. & Stark, H. Role of cytochrome P450 polymorphisms and functions in
577 development of ulcerative colitis. *World J Gastroenterol* **25**, 2846 (2019).
578 29. Dubuquoy, L. *et al.* PPARγ as a new therapeutic target in inflammatory bowel diseases.
579 *Gut* **55**, 1341 (2006).
580 30. Ashton, J. J. *et al.* Deleterious Genetic Variation Across the NOD Signaling Pathway Is
581 Associated With Reduced NFKB Signaling Transcription and Upregulation of Alternative
582 Inflammatory Transcripts in Pediatric Inflammatory Bowel Disease. *Inflamm Bowel Dis*
583 **28**, 912–922 (2022).
584 31. Lim, S. M. *et al.* The effect of the menstrual cycle on inflammatory bowel disease: A
585 prospective study. *Gut Liver* **7**, 51–57 (2013).

586 32. Chomarat, P., Banchereau, J., Davoust, J. & Karolina Palucka, A. IL-6 switches the
587 differentiation of monocytes from dendritic cells to macrophages. *Nature Immunology*
588 *2000 1:6* **1**, 510–514 (2000).
589 33. Murphy, C. C. & Zaki, T. A. Changing epidemiology of colorectal cancer — birth cohort
590 effects and emerging risk factors. *Nat Rev Gastroenterol Hepatol* **21**, 25–34 (2023).
591 34. Schmitt, M. & Greten, F. R. The inflammatory pathogenesis of colorectal cancer. *Nat Rev*
592 *Immunol* **21**, 653–667 (2021).
593 35. Herzig, M., Savarese, F., Novatchkova, M., Semb, H. & Christofori, G. Tumor progression
594 induced by the loss of E-cadherin independent of β-catenin/Tcf-mediated Wnt signaling.
595 *Oncogene* **26**, 2290–2298 (2007).
596 36. Zink, D., Fischer, A. H. & Nickerson, J. A. Nuclear structure in cancer cells. *Nature*
597 *Reviews Cancer 2004 4:9* **4**, 677–687 (2004).
598 37. Michl, J., White, B., Monterisi, S., Bodmer, W. F. & Swietach, P. Phenotypic screen of
599 sixty-eight colorectal cancer cell lines identifies CEACAM6 and CEACAM5 as markers of
600 acid resistance. *Proc Natl Acad Sci U S A* **121**, e2319055121 (2024).
601 38. Goodman, W. A., Erkkila, I. P. & Pizarro, T. T. Sex matters: impact on pathogenesis,
602 presentation and treatment of inflammatory bowel disease. *Nature Reviews*
603 *Gastroenterology & Hepatology 2020 17:12* **17**, 740–754 (2020).
604 39. D'Alessio, S. *et al.* Revisiting fibrosis in inflammatory bowel disease: the gut thickens. *Nat*
605 *Rev Gastroenterol Hepatol* **19**, 169–184 (2022).
606 40. Ryan, F. J. *et al.* Colonic microbiota is associated with inflammation and host epigenomic
607 alterations in inflammatory bowel disease. *Nat Commun* **11**, 1–12 (2020).
608 41. Mendelson, S., Anbukkarasu, P., Cassisi, J. E. & Zaman, W. Gastrointestinal functioning
609 and menstrual cycle phase in emerging young adult women: a cross-sectional study.
610 *BMC Gastroenterol* **23**, 1–10 (2023).
611 42. Bellofiore, N., Ellery, S., Mamrot, J., … D. W.-A. journal of & 2017, undefined. First
612 evidence of a menstruating rodent: the spiny mouse (Acomys cahirinus). *Elsevier*.
613 43. Bellofiore, N., Cousins, F., Temple-Smith, P., Dickinson, H. & Evans, J. A missing piece:
614 the spiny mouse and the puzzle of menstruating species. *J Mol Endocrinol* **61**, R25–R41
615 (2018).
616 44. Onji, M. *et al.* RANK drives structured intestinal epithelial expansion during pregnancy.
617 *Nature 2024 637:8044* **637**, 156–166 (2024).
618 45. Ameku, T. *et al.* Growth of the maternal intestine during reproduction. *Cell* **0**, (2025).

619 46. Paone, P. & Cani, P. D. Mucus barrier, mucins and gut microbiota: the expected slimy
620 partners? *Gut* **69**, 2232 (2020).
621 47. Aust, D. E. *et al.* Altered distribution of β-catenin, and its binding proteins E-cadherin and
622 APC, in ulcerative colitis-related colorectal cancers. *Modern Pathology* **14**, 29–39 (2001).
623 48. Winton, D. J. & Ponder, B. A. J. Stem-cell organization in mouse small intestine. *Proc Biol*
624 *Sci* **241**, 13–18 (1990).
625 49. Winawer, S. J. *et al.* Colorectal Cancer Screening: Clinical Guidelines and Rationale The
626 Adenoma-Carcinoma Sequence. *Gastroenterology* **112**, 594–642 (1997).
627 50. Gillen, C. D., Walmsley, R. S., Prior, P., Andrews, H. A. & Allan, R. N. Ulcerative colitis
628 and Crohn's disease: a comparison of the colorectal cancer risk in extensive colitis. *Gut*
629 **35**, 1590 (1994).
630 51. Lee, S. H. *et al.* Apposition of Fibroblasts With Metaplastic Gastric Cells Promotes
631 Dysplastic Transition. *Gastroenterology* **165**, 374–390 (2023).
632 52. Pizarro, T. T. *et al.* Challenges in IBD Research: Preclinical Human IBD Mechanisms.
633 *Inflamm Bowel Dis* **25**, S5–S12 (2019).
634 53. Heller, C. A. *et al.* Challenges in IBD Research. *Inflamm Bowel Dis* **25**, S31–S39 (2019).
635 54. Jalili-Firoozinezhad, S. *et al.* A complex human gut microbiome cultured in an anaerobic
636 intestine-on-a-chip. *Nat Biomed Eng* **3**, 520–531 (2019).
637 55. Kasendra, M. *et al.* Development of a primary human Small Intestine-on-a-Chip using
638 biopsy-derived organoids. *Sci Rep* **8**, 1–14 (2018).
639 56. Bein, A. *et al.* Nutritional deficiency in an intestine-on-a-chip recapitulates injury hallmarks
640 associated with environmental enteric dysfunction. *Nat Biomed Eng* **6**, 1236–1247
641 (2022).
642 57. Aden, K. *et al.* BASIC AND TRANSLATIONAL-ALIMENTARY TRACT Metabolic
643 Functions of Gut Microbes Associate With Efficacy of Tumor Necrosis Factor Antagonists
644 in Patients With Inflammatory Bowel Diseases. (2019) doi:10.1053/j.gastro.2019.07.025.
645 58. Kennedy, M. S. *et al.* Diet outperforms microbial transplant to drive microbiome recovery
646 in mice. *Nature 2025* 1–9 (2025) doi:10.1038/s41586-025-08937-9.
647 59. Vieujean, S. *et al.* Understanding the therapeutic toolkit for inflammatory bowel disease.
648 *Nature Reviews Gastroenterology & Hepatology 2025 22:6* **22**, 371–394 (2025).
649 60. Kim, H. J., Huh, D., Hamilton, G. & Ingber, D. E. Human gut-on-a-chip inhabited by
650 microbial flora that experiences intestinal peristalsis-like motions and flow. *Lab Chip* **12**,
651 2165–2174 (2012).

652 61. Tovaglieri, A. *et al.* Species-specific enhancement of enterohemorrhagic E. coli
653 pathogenesis mediated by microbiome metabolites. *Microbiome* **7**, 1–21 (2019).
654 62. Turco, M. Y. *et al.* Long-term, hormone-responsive organoid cultures of human
655 endometrium in a chemically defined medium. *Nat Cell Biol* **19**, 568–577 (2017).
656 63. Gnecco, J. S. *et al.* Organoid co-culture model of the human endometrium in a fully
657 synthetic extracellular matrix enables the study of epithelial-stromal crosstalk. *Med* **4**,
658 554-579.e9 (2023).
659 64. Li, H. & Durbin, R. Fast and accurate short read alignment with Burrows–Wheeler
660 transform. *Bioinformatics* **25**, 1754–1760 (2009).
661 65. Genomics in the Cloud: Using Docker, GATK, and WDL in Terra - Geraldine A. Van der
662 Auwera, Brian D. O'Connor - Google Books.
663 https://books.google.com/books?hl=en&lr=&id=vsXaDwAAQBAJ&oi=fnd&pg=PP1&dq=V
664 an+der+Auwera+GA+%26+O%27Connor+BD.+(2020).+Genomics+in+the+Cloud:+Using
665 +Docker,+GATK,+and+WDL+in+Terra+(1st+Edition).+O%27Reilly+Media.&ots=5lcr0E-
666 qna&sig=43MTbQQNO_yexxB7NxDgVt88kOk#v=onepage&q&f=false.
667 66. Poell, J. B. *et al.* ACE: absolute copy number estimation from low-coverage whole-
668 genome sequencing data. *Bioinformatics* **35**, 2847–2849 (2019).
669 67. Scheinin, I. *et al.* DNA copy number analysis of fresh and formalin-fixed specimens by
670 shallow whole-genome sequencing with identification and exclusion of problematic
671 regions in the genome assembly. *Genome Res* **24**, 2022–2032 (2014).
672
673

674 **Figure Legends**

675 **Figure 1: Primary human Colon Chips generated with epithelium and fibroblasts**
676 **isolated from Healthy and IBD patient samples. A)** Photograph of the commercially available
677 Organ Chip device (left) and a cross-sectional illustration of the epithelial-stromal tissue
678 interface (right) formed with patient-derived cells, which is composed of a fibroblast rich stroma
679 that is perfused with medium to mimic interstitial fluid flow separated by a flexible, porous, ECM-
680 coated membrane from a colon epithelium above. The epithelium, which is composed of
681 absorptive cells and Goblet cells, secretes a thick mucus layer into the lumen of the apical
682 channel that also experiences fluid flow. The entire tissue-tissue interface can be stretched and
683 relaxed rhythmically to mimic peristalsis-like motions by applying cyclic suction to hollow side
684 chambers in the flexible device (not shown). **B)** Height of crypts formed in Colon Chips
685 measured at 11 days. Numbers indicate *P* values between compared groups, as determined by
686 one-way ANOVA test (n=3 Healthy, green; 2 CD, magenta; and 2 UC, cyan). **C)** Representative
687 bright field microscopic images of Healthy and IBD Chips created with cells from CD or UC
688 patients viewed from above on day 3, 7, and 11. A functional epithelial monolayer progressively
689 accumulated mucus, which appears as opaque blackened fuzzy material, in the apical channel
690 of all chips over the 11 day time course; however, mucus accumulation was suppressed in the
691 IBD Chips with the UC Chips displaying a greater reduction (bar, 500 μm)**. D)** Brightfield image
692 of vertical cross-sections through healthy and IBD Colon chips showing that the crypt-like
693 epithelial structures are shorter in the CD and UC Colon Chips (bar, 100 μm)**. E)** Histological
694 H&E stained vertical cross-sections through healthy and IBD Colon chips confirming the
695 presence of columnar colon epithelium containing goblet cells in healthy epithelium, and a
696 significant reduction in the height of the epithelial monolayer with reduced numbers of goblet
697 cells in the IBD Chips (bar, 50 μm). **F)** Immunofluorescence microscopic views showing
698 distribution of SOX9 and CK20 in crypts in the colon epithelium of Healthy and IBD Chips (bar,

699 50 μm). **G**) Inflammatory cytokine protein levels measured in the basal outflows of Healthy (H)
700 and IBD Chips on culture day 11 (n = 3-5 chips/ condition; chips were created with cells from 3
701 healthy (green), 2 CD (magenta), and 2 UC (cyan) patient donors, with each symbol represents
702 a chip created with cells from a different patient. Numbers indicate *P* values between compared
703 groups, as determined by two-tailed student's t-test. All data represent mean ± SD; *p* values are
704 shown in all figures. Source data and statistical tests are provided as a Source Data file.

705 **Figure 2: Peristalsis-like cyclic strain influences mucus production and fibrosis in**
706 **Colon Chips. A)** Representative side-view images microscopy of Healthy or IBD Chips with (+)
707 and without (-) exposure to mechanical deformations visualizing mucus layer accumulation
708 (white diffuse material) in Healthy Chips using dark-field microscopy. Note that limited mucus
709 was produced by IBD epithelium (bar, 1 mm). **B)** Quantification of the height of the mucus layer
710 overlying Healthy and IBD epithelium on-chip when cultured under the conditions in A. Numbers
711 indicate *P* values between compared groups, as determined by one-way ANOVA test. (n = 3
712 healthy, green; 2 CD, magenta; and 2 UC, cyan). **C)** Heat map of genes showing that
713 peristalsis-like mechanical stimulation (+) increases expression of genes related to mucus
714 production in Healthy Chips, but not IBD Chips (n = 3 healthy, 1 CD and 2 UC). **D)** Second
715 harmonic microscopic images of the fibroblast stroma in Healthy versus IBD Chips showing
716 greater collagen fibril accumulation (green) with mechanical strain (+ Strain) in both chips, and
717 that this response is greatly accentuated in IBD Chips (bar, 200 μm). **E)** Collagen fibril signal
718 intensity in the stroma of Healthy versus IBD Chips quantified in second harmonic microscopic
719 images. Numbers indicate *P* values between compared groups, as determined by one-way
720 ANOVA test (n = 3 healthy, green; 2 CD, magenta; and 2 UC, cyan). **F)** Heat map of genes
721 showing that peristalsis-like cyclic strain enhances expression of genes associated with fibrillar
722 collagen production in IBD fibroblasts, but not in healthy fibroblasts (n = 3 healthy, 1 CD and 2
723 UC). **G)** Heat maps of showing that cyclic strain enhances greater expression of IBD-associated
724 inflammatory genes in IBD Chips compared to Healthy Chips both in epithelium and fibroblasts

725 (n=3 Healthy, 1 CD, and 2 UC). Source data and statistical tests are provided as a Source Data
726 file.

727 **Figure 3: Effects of ovarian hormones in Female Colon Chips.** DIC images from
728 above (**A**) and vertical cross-sectional views of confocal microscopic images (**B**) of healthy and
729 IBD Chips 7 days post treatment with exposure to E2, E2 plus MPA, or PAH.. **A**) When viewed
730 from above, exposure to PAH appeared to slightly increase the density of crypt-like structures in
731 both healthy and IBD chips (bar, 500 μm). **B)** When viewed in vertical cross-sections, the
732 number and height of crypt-like structures increased when exposed to PAH as well as E2+MPA
733 in both Healthy and IBD Chips, although the scale of the response was much less in the IBD
734 Chips (bar, 100 μm; magenta: phalloidin, cyan: DAPI; dashed white line, upper surface of chip
735 membrane; dashed yellow line, upper luminal boundary of the crypt). **C)** Quantification of
736 heights of crypt-like structures in Healthy and IBD Chips in the presence or absence of different
737 combinations of the ovarian hormones (E2, MPA, and PAH), as indicated (n=8-12 chips of 2
738 healthy, 1 CD and 2 UC patients from at least 2 independent experiments). **D)** Second harmonic
739 microscopic images of fibrillar collagen (green) produced by fibroblasts in response to the
740 different hormonal conditions shown in A and B demonstrating a much greater fibrosis response
741 in the IBD Chips compared to Healthy when exposed to pregnancy mimiking hormone
742 combination (E2+MPA+PAH) (bar, 200 μm; n=4-6 chips of 1 CD, 2 UC and 2 Healthy each from
743 2 independent experiments). **E)** Graphs showing quantification of collagen fibril signal intensity
744 in the stroma of Healthy versus IBD Chips using second harmonic microscopic imaging
745 (numbers indicate *P* values between compared groups, as determined by one-way ANOVA test;
746 n=8-12 chips of 2 healthy, 1 CD and 2 UC patients from at least 2 independent experiments). **F)**
747 Heatmaps showing production of pro-inflammatory cytokine and chemokine proteins in apical
748 (epithelial) and basal (fibroblast) channels of Healthy versus IBD Chips 7 days post treatment
749 with different female hormone exposures, as indicated. Note that exposure to female hormones
750 significantly increased expression of inflammatory factors in both the epithelium and fibroblasts

751 in IBD Chips whereas they suppressed their production in Healthy Chips (numbers indicate
752 *P* values between compared groups, as determined by one-tailed student's t-test; all data
753 represent mean ± SD). Source data and statistical tests are provided as a Source Data file; *p*
754 values are shown in all figures.
755
756 **Figure 4: Tissue recombinant chips reveal that the IBD fibroblasts drive**
757 **compromise of the permeability barrier and inflammation in the epithelium**. **A)** Graphs
758 showing that intestinal barrier permeability to cascade blue is much higher in homotypic IBD
759 Chips compared to Healthy Chips and that tissue recombinants of IBD fibroblasts with healthy
760 (H) epithelium results in a similar high level of barrier compromise on-chip. This is not observed
761 in the IBD or healthy epithelium in the absence of fibroblasts or in IBD epithelium with healthy
762 fibroblasts. Numbers indicate *P* values between compared groups, as determined by one-way
763 ANOVA test (n = 3 healthy, green; 2 CD, magenta; and 2 UC, cyan). **B)** Quantification of
764 cytokine protein levels revealed that combination of IBD fibroblasts with healthy epithelium
765 results in increased production of IL-6 and MCP-1 in Colon Chips, whereas this was not seen in
766 healthy epithelium alone or homotypic Colon Chips. Numbers indicate *P* values between
767 compared groups, as determined by one-way ANOVA test (n = 3 healthy, green; 1 CD,
768 magenta; and 2 UC, cyan). **C)** IL-6 and MCP-1 production by IBD epithelium also required the
769 presence of IBD fibroblasts. Numbers indicate *P* values between compared groups, as
770 determined by one-way ANOVA test (n = 3 healthy, green; 1 CD, magenta; and 2 UC, cyan). **D)**
771 Peristalsis-like cyclic strain preferentially stimulates migration of PBMCs (magenta) from the
772 fibroblast stroma in the basal channel (Basal) to the epithelium in the apical channel (Apical) in
773 IBD Chips but not in heterotypic chips with IBD epithelium and healthy fibroblasts or in Healthy
774 Chips. **E)** Quantification of the results from **D** confirmed that IBD Chips exhibited higher baseline
775 recruitment of PBMCs to the surface of the fibroblast stroma in the basal channel and that this
776 was not altered by mechanical strain, whereas IBD epithelium combined with healthy stroma or

777 Healthy Chips only displayed significantly less PBMC recruitment. In contrast, the number of
778 PBMCs that migrated to the epithelium in the Apical channel more than doubled in IBD Chips
779 when they were exposed to peristalsis-like mechanical deformations, and overall migration of
780 PBMCs was minimal when IBD fibroblasts were absent. Numbers indicate *P* values between
781 compared groups, as determined by one-way ANOVA test (n = 2 healthy, green; 1 CD,
782 magenta; and 1 UC, cyan). Source data and statistical tests are provided as a Source Data file.

783 **Figure 5: Exposure to carcinogen preferentially promotes mutagenesis and early**
784 **steps in carcinogenesis in IBD Chips. A)** DIC images of the epithelium when viewed from
785 above in Healthy (H) and IBD Chips after 21 days of culture in the presence or absence of the
786 carcinogen (ENU) showing that undulating crypt-like structures are lost in both Healthy and IBD
787 Chips after exposure to ENU (bar, 500 μm). **B)** Quantification of results from **A** showing that
788 ENU decreases height of the epithelium in both healthy and IBD Colon Chips. Numbers indicate
789 *P* values between compared groups, as determined by one-way ANOVA test (n = 3 healthy,
790 green; 2 CD, magenta; and 2 UC, cyan). **C)** Epithelial barrier permeability increased as a result
791 of exposure to ENU in Healthy and IBD Chips. Numbers indicate *P* values between compared
792 groups, as determined by one-way ANOVA test. (n = 3 healthy, green; 2 CD, magenta; and 2
793 UC, cyan). **D)** Heatmaps showing inflammatory cytokine protein levels measured in outflows
794 from the apical channel of Healthy and IBD Chips 3 weeks post-ENU exposure. Importantly,
795 ENU exposure significantly increased inflammatory cytokine production in IBD Chips made with
796 cells from both CD and UC patients compared to healthy patients. **E)** Confocal microscopic top-
797 view images showing β-catenin and E-cadherin localization and nuclear staining (DAPI) in the
798 epithelium within Healthy and IBD Chips 3 weeks post-ENU exposure (bar, 20 μm). **F)**
799 Quantification of protein staining intensity and morphology reveal that ENU exposure decreases
800 E-cadherin levels and increases nuclear localization of β-catenin in IBD patient-derived Colon
801 Chips compared to Healthy Chips. ENU exposure also resulted in greater nucleus size and less

802 roundness. Numbers indicate *P* values between compared groups, as determined by Student's
803 t-test (n = 3 healthy, green; 2 CD, magenta; and 2 UC, cyan). **G)** Plots showing copy number
804 changes across all human chromosomes in Healthy and IBD Chips pre- (red) and 3 weeks post-
805 ENU exposure (blue). Green bars indicate amplification of gene sequences for the whole
806 chromosome. Each symbol represents an individual Healthy or IBD patient-derived chip. **H)**
807 Confocal microscopic top-view images showing early stage CRC marker, CEACAM5,
808 expression in healthy and IBD epithelium when they are cultured with with or without healthy
809 fibroblasts or IBD fibroblasts and exposed to ENU for 3 weeks. Source data and statistical tests
810 are provided as a Source Data file.

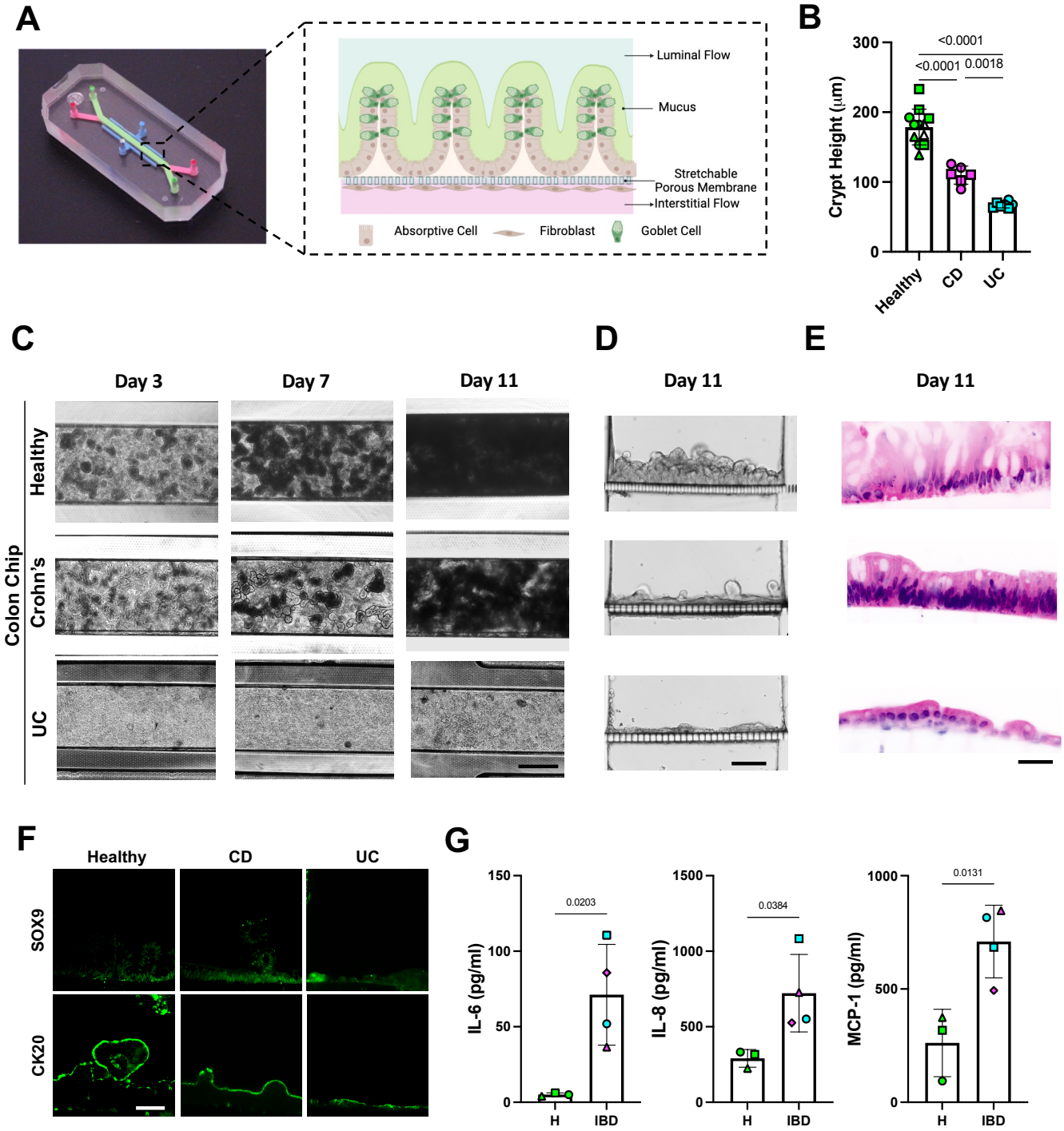
A
Luminal Flow
Mucus
Stretchable Porous Membrane
Interstitial Flow
Absorptive Cell
Fibroblast
Goblet Cell
B
Crypt Height (μm)
300
200
100
0
<0.0001
<0.0001
0.0018
Healthy
CD
UC
C
Day 3
Day 7
Day 11
Colon Chip
Healthy
Crohn's
UC
D
Day 11
E
Day 11
F
Healthy
CD
UC
SOX9
CK20
G
IL-6 (pg/ml)
150
100
50
0
0.0203
H
IBD
IL-8 (pg/ml)
1500
1000
500
0
0.0384
H
IBD
MCP-1 (pg/ml)
1000
500
0
0.0131
H
IBD

Fig. 1

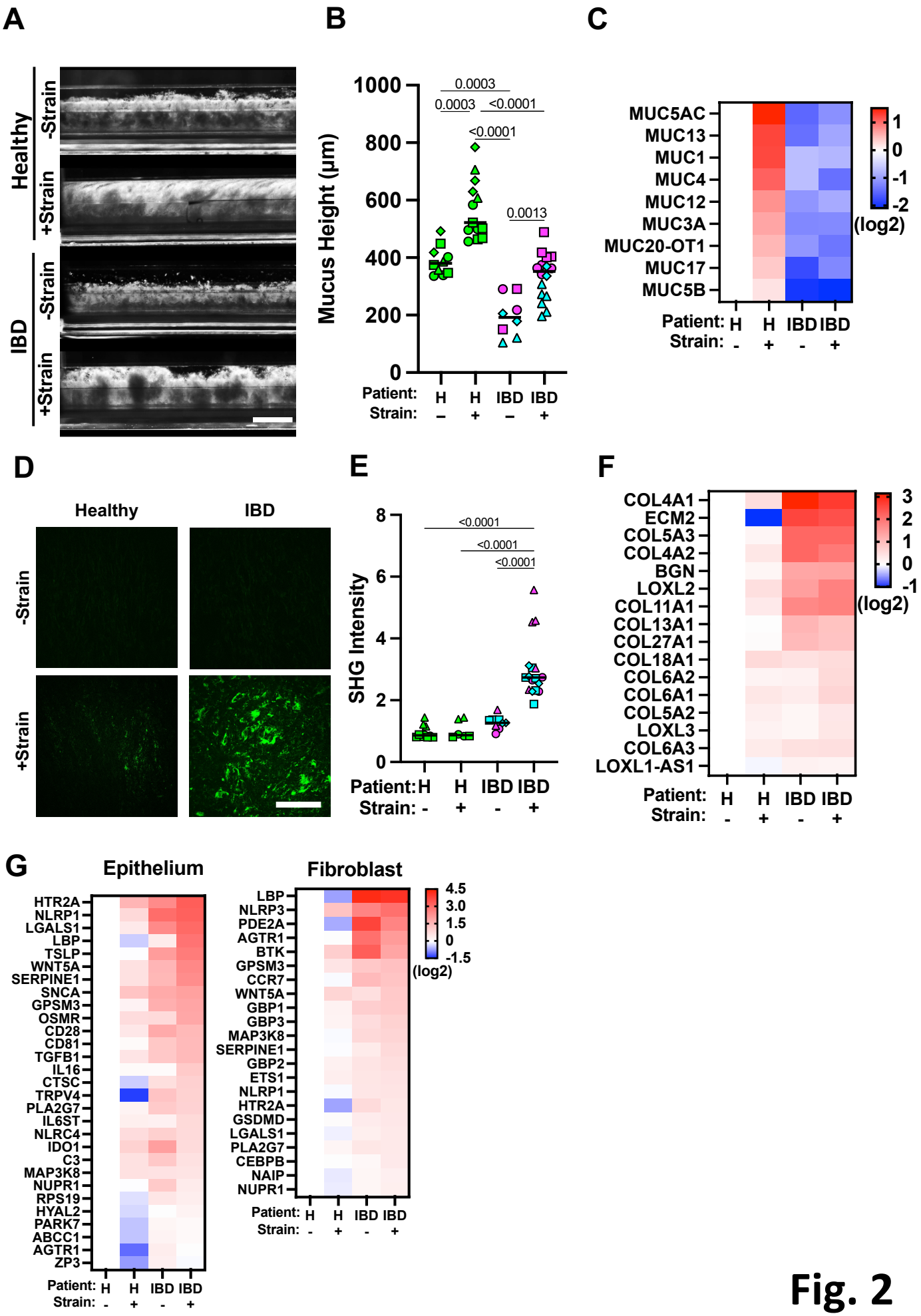
A
Healthy
-Strain
+Strain
IBD
-Strain
+Strain
B
Mucus Height (µm)
1000
800
600
400
200
0
0.0003
0.0003
<0.0001
<0.0001
0.0013
Patient: H H IBD IBD
Strain: – + – +
C
MUC5AC
MUC13
MUC1
MUC4
MUC12
MUC3A
MUC20-OT1
MUC17
MUC5B
1
0
-1
-2
(log2)
Patient: H H IBD IBD
Strain: - + - +
D
Healthy
IBD
-Strain
+Strain
E
SHG Intensity
8
6
4
2
0
<0.0001
<0.0001
<0.0001
Patient: H H IBD IBD
Strain: - + - +
F
COL4A1
ECM2
COL5A3
COL4A2
BGN
LOXL2
COL11A1
COL13A1
COL27A1
COL18A1
COL6A2
COL6A1
COL5A2
LOXL3
COL6A3
LOXL1-AS1
3
2
1
0
-1
(log2)
Patient: H H IBD IBD
Strain: - + - +
G
Epithelium
HTR2A
NLRP1
LGALS1
LBP
TSLP
WNT5A
SERPINE1
SNCA
GPSM3
OSMR
CD28
CD81
TGFB1
IL16
CTSC
TRPV4
PLA2G7
IL6ST
NLRC4
IDO1
C3
MAP3K8
NUPR1
RPS19
HYAL2
PARK7
ABCC1
AGTR1
ZP3
Patient: H H IBD IBD
Strain: - + - +
Fibroblast
LBP
NLRP3
PDE2A
AGTR1
BTK
GPSM3
CCR7
WNT5A
GBP1
GBP3
MAP3K8
SERPINE1
GBP2
ETS1
NLRP1
HTR2A
GSDMD
LGALS1
PLA2G7
CEBPB
NAIP
NUPR1
4.5
3.0
1.5
0
-1.5
(log2)
Patient: H H IBD IBD
Strain: - + - +

Fig. 2

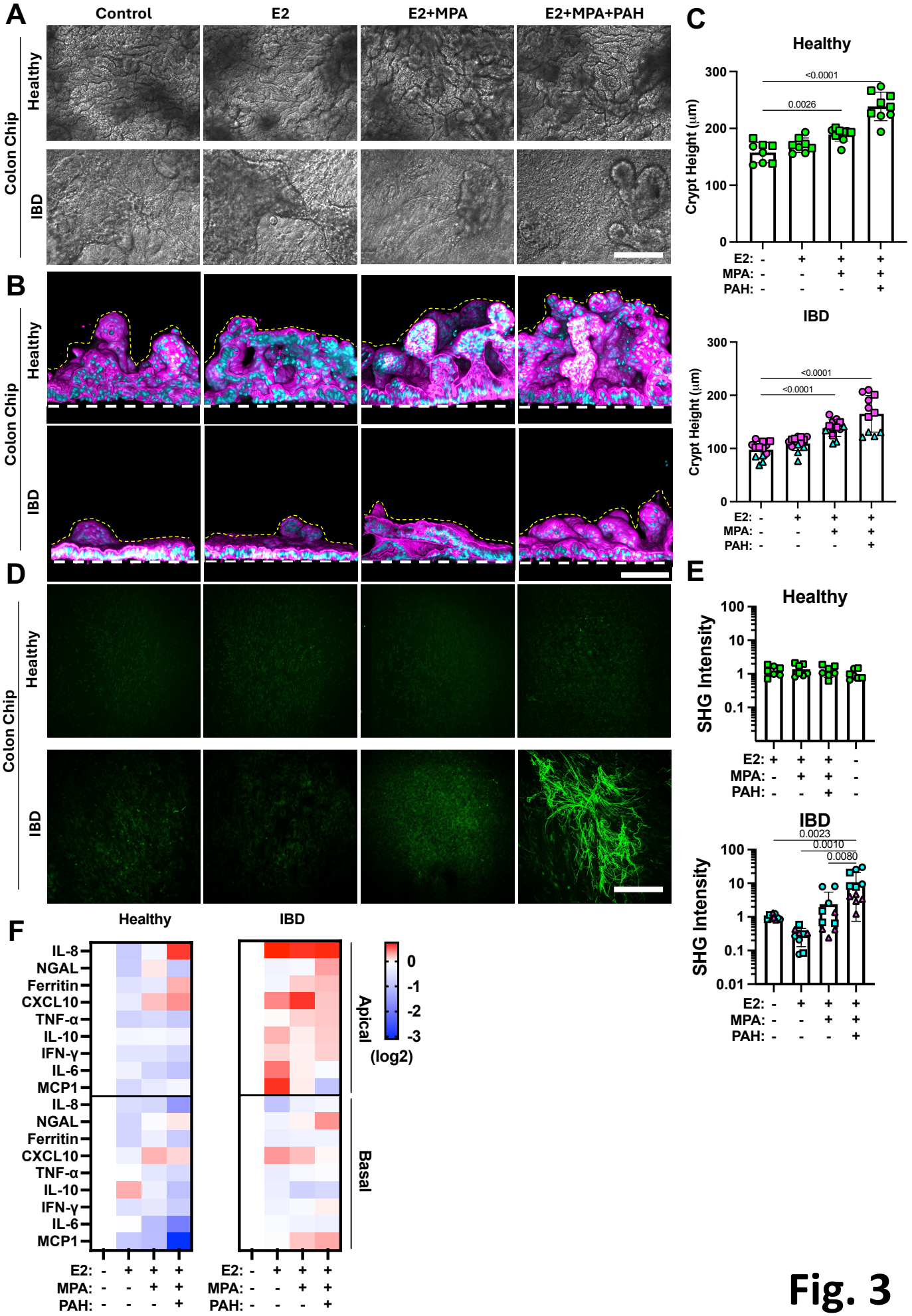
A
Control
E2
E2+MPA
E2+MPA+PAH
Colon Chip
Healthy
IBD
B
Colon Chip
Healthy
IBD
C
Healthy
Crypt Height (μm)
300
200
100
0
<0.0001
0.0026
E2: - + + +
MPA: - - + +
PAH: - - - +
IBD
Crypt Height (μm)
300
200
100
0
<0.0001
<0.0001
E2: - + + +
MPA: - - + +
PAH: - - - +
D
Colon Chip
Healthy
IBD
E
Healthy
SHG Intensity
100
10
1
0.1
E2: + + + -
MPA: - + + -
PAH: - - + -
IBD
SHG Intensity
100
10
1
0.1
0.01
0.0023
0.0010
0.0080
E2: - + + +
MPA: - - + +
PAH: - - - +
F
Healthy
IBD
IL-8
NGAL
Ferritin
CXCL10
TNF-α
IL-10
IFN-γ
IL-6
MCP1
Apical
Basal
0
-1
-2
-3
(log2)
E2: - + + +
MPA: - - + +
PAH: - - - +
E2: - + + +
MPA: - - + +
PAH: - - - +

Fig. 3

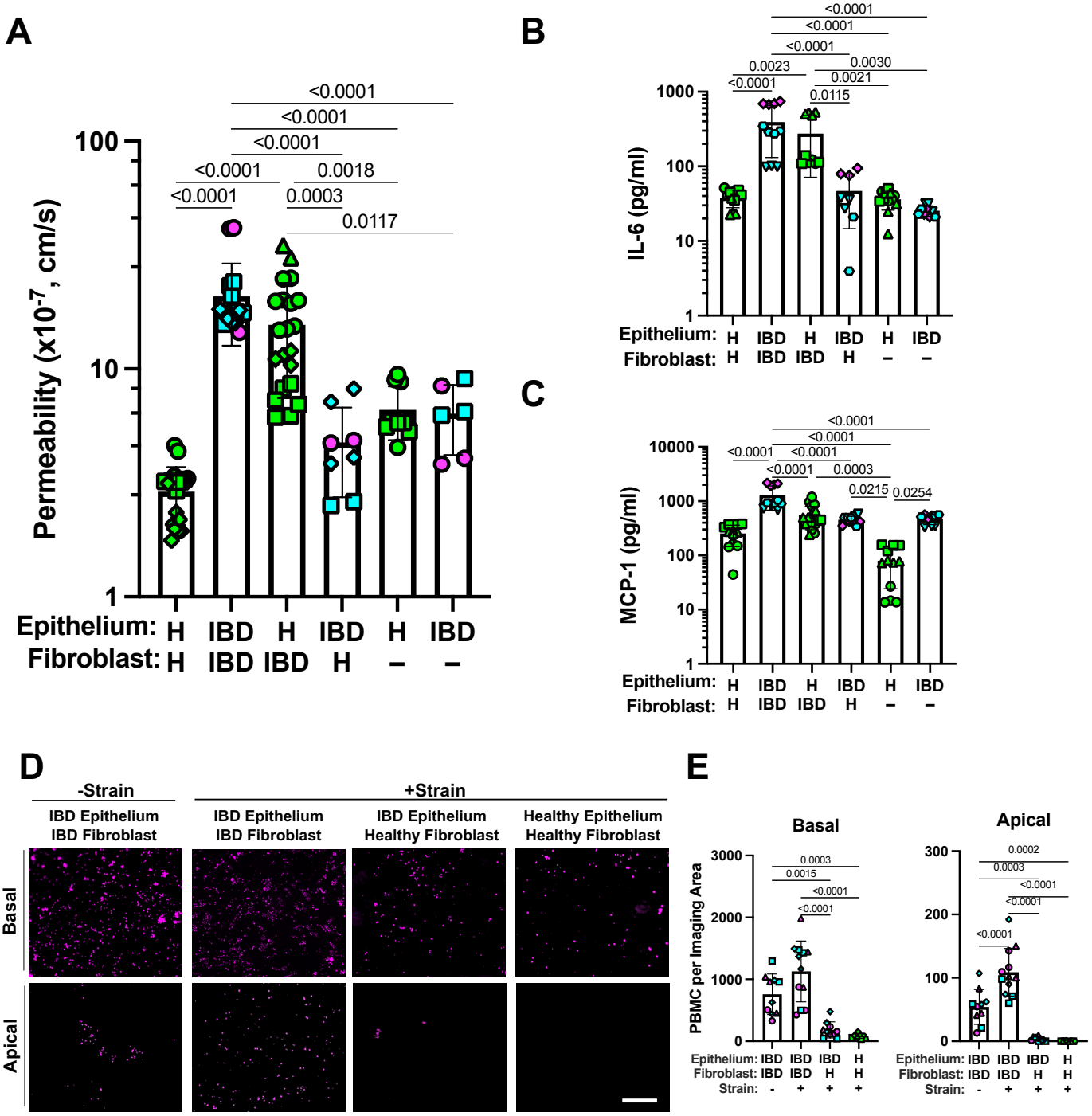
A
Permeability (x10-7, cm/s)
100
10
1
<0.0001
<0.0001
<0.0001
<0.0001
<0.0001
0.0018
0.0003
0.0117
Epithelium: H IBD H IBD H IBD
Fibroblast: H IBD IBD H – –
B
IL-6 (pg/ml)
1000
100
10
1
<0.0001
<0.0001
<0.0001
0.0023
<0.0001
0.0030
0.0021
0.0115
Epithelium: H IBD H IBD H IBD
Fibroblast: H IBD IBD H – –
C
MCP-1 (pg/ml)
10000
1000
100
10
1
<0.0001
<0.0001
<0.0001
<0.0001
<0.0001
<0.0001
0.0003
0.0215
0.0254
Epithelium: H IBD H IBD H IBD
Fibroblast: H IBD IBD H – –
D
-Strain
+Strain
IBD Epithelium IBD Fibroblast
IBD Epithelium IBD Fibroblast
IBD Epithelium Healthy Fibroblast
Healthy Epithelium Healthy Fibroblast
Basal
Apical
E
Basal
Apical
PBMC per Imaging Area
3000
2000
1000
0
300
200
100
0
0.0003
0.0015
<0.0001
<0.0001
0.0002
0.0003
<0.0001
<0.0001
<0.0001
Epithelium: IBD IBD IBD H
Fibroblast: IBD IBD H H
Strain: - + + +

Fig. 4

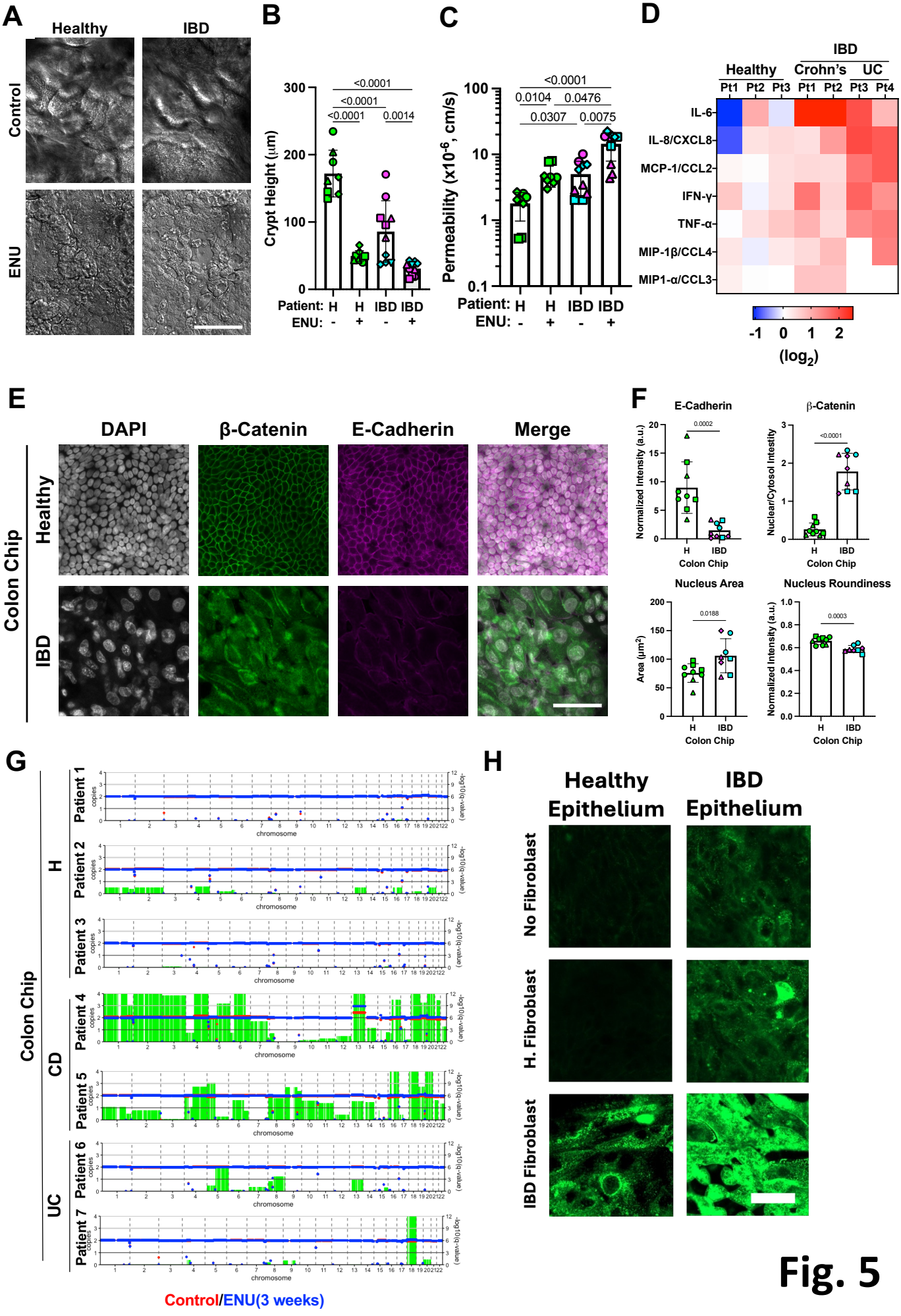
A
Healthy
IBD
Control
ENU
B
Crypt Height (μm)
<0.0001
<0.0001
<0.0001
0.0014
Patient: H H IBD IBD
ENU: - + - +
C
Permeability (x10-6, cm/s)
<0.0001
0.0104
0.0476
0.0307
0.0075
Patient: H H IBD IBD
ENU: - + - +
D
IBD
Healthy
Crohn's
UC
Pt1 Pt2 Pt3 Pt1 Pt2 Pt3 Pt4
IL-6
IL-8/CXCL8
MCP-1/CCL2
IFN-γ
TNF-α
MIP-1β/CCL4
MIP1-α/CCL3
-1 0 1 2
(log2)
E
DAPI
β-Catenin
E-Cadherin
Merge
Colon Chip
Healthy
IBD
F
E-Cadherin
β-Catenin
Normalized Intensity (a.u.)
Nuclear/Cytosol Intestity
0.0002
<0.0001
H IBD
Colon Chip
Nucleus Area
Nucleus Roundiness
Area (μm2)
0.0188
0.0003
G
Colon Chip
H
CD
UC
Patient 1
Patient 2
Patient 3
Patient 4
Patient 5
Patient 6
Patient 7
copies
chromosome
-log10(q-value)
Control/ENU(3 weeks)
H
Healthy Epithelium
IBD Epithelium
No Fibroblast
H. Fibroblast
IBD Fibroblast

Fig. 5

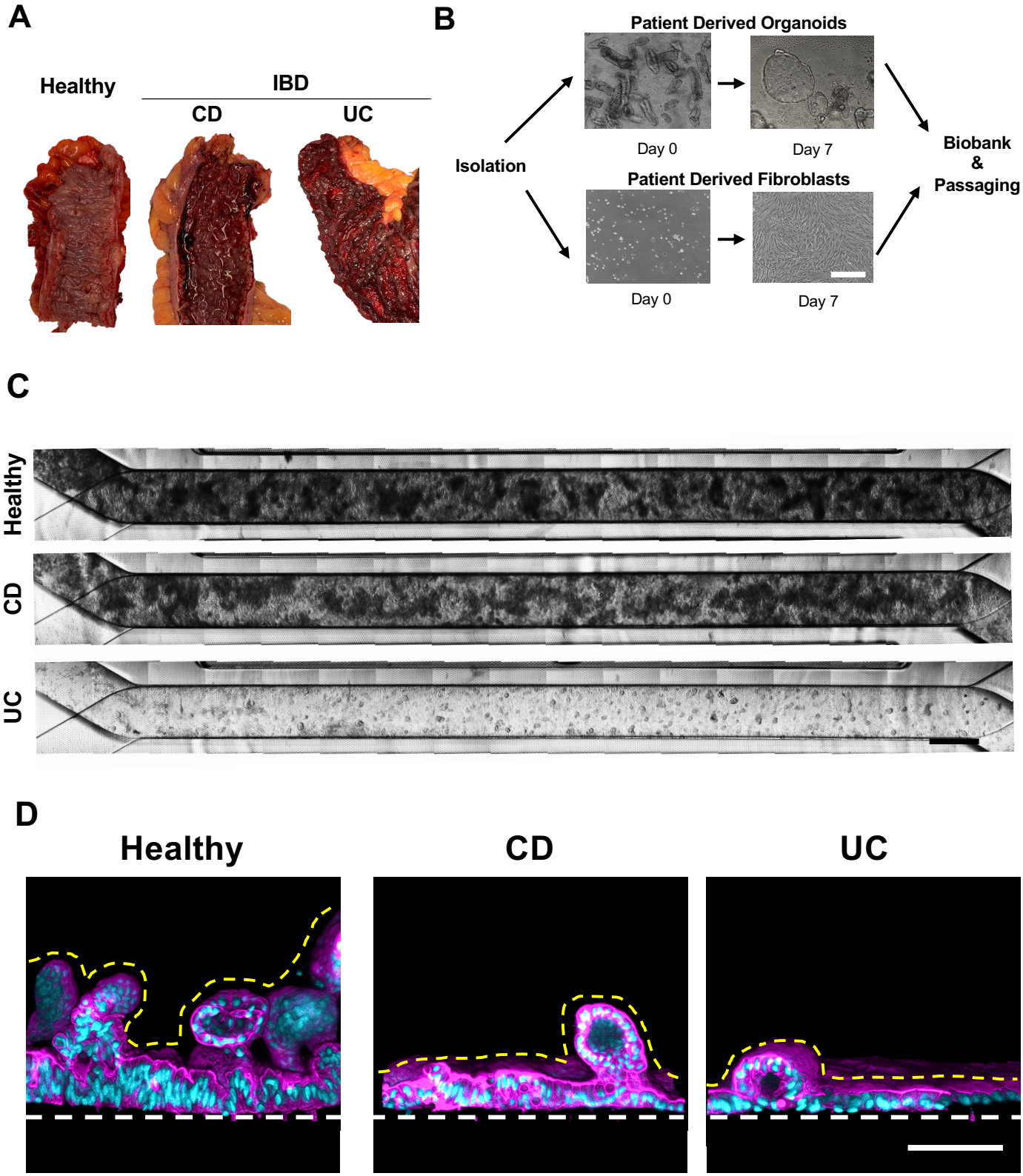

Extended Data Fig. 1

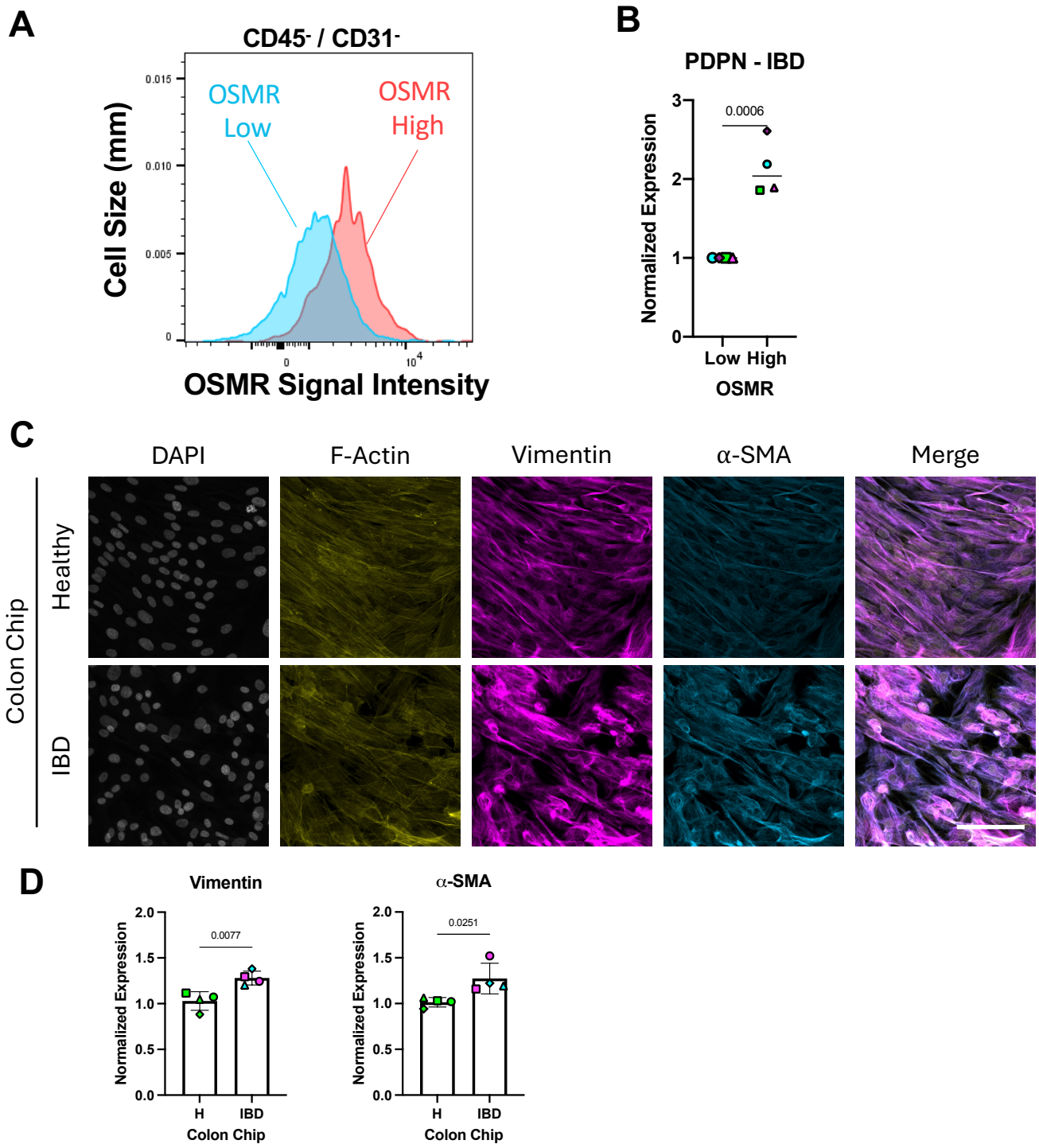

Extended Data Fig. 2

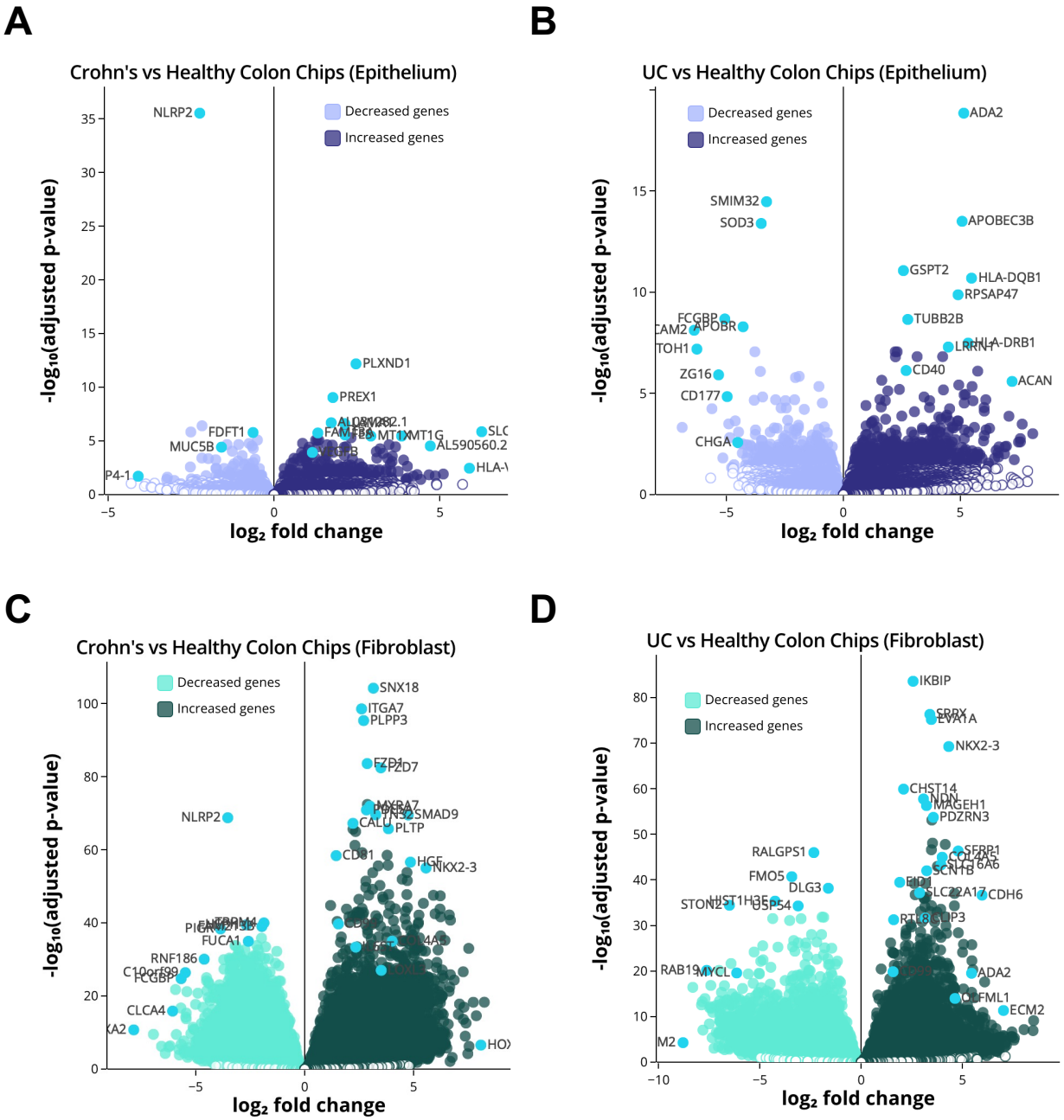

Extended Data Fig. 3

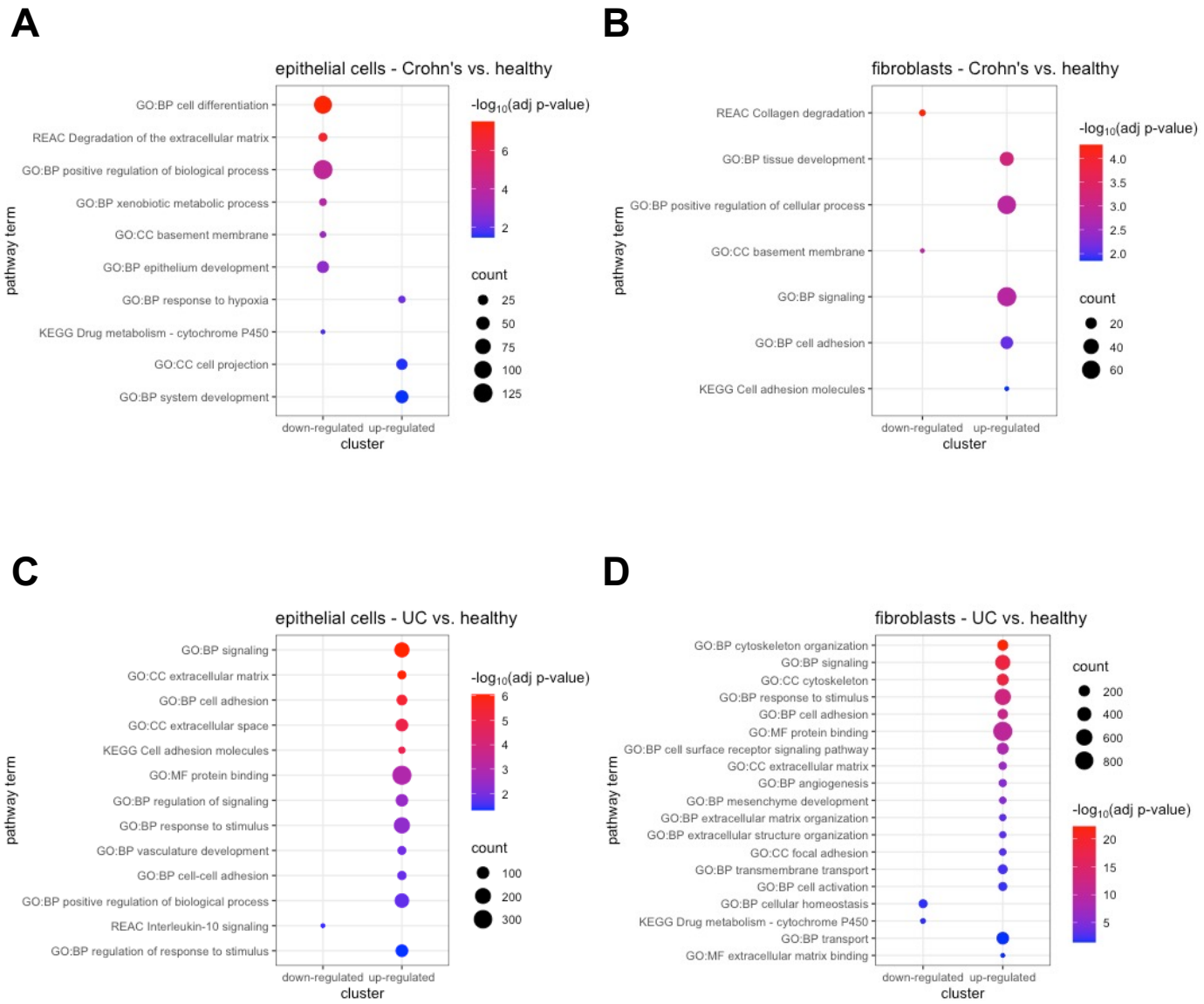

Extended Data Fig. 4

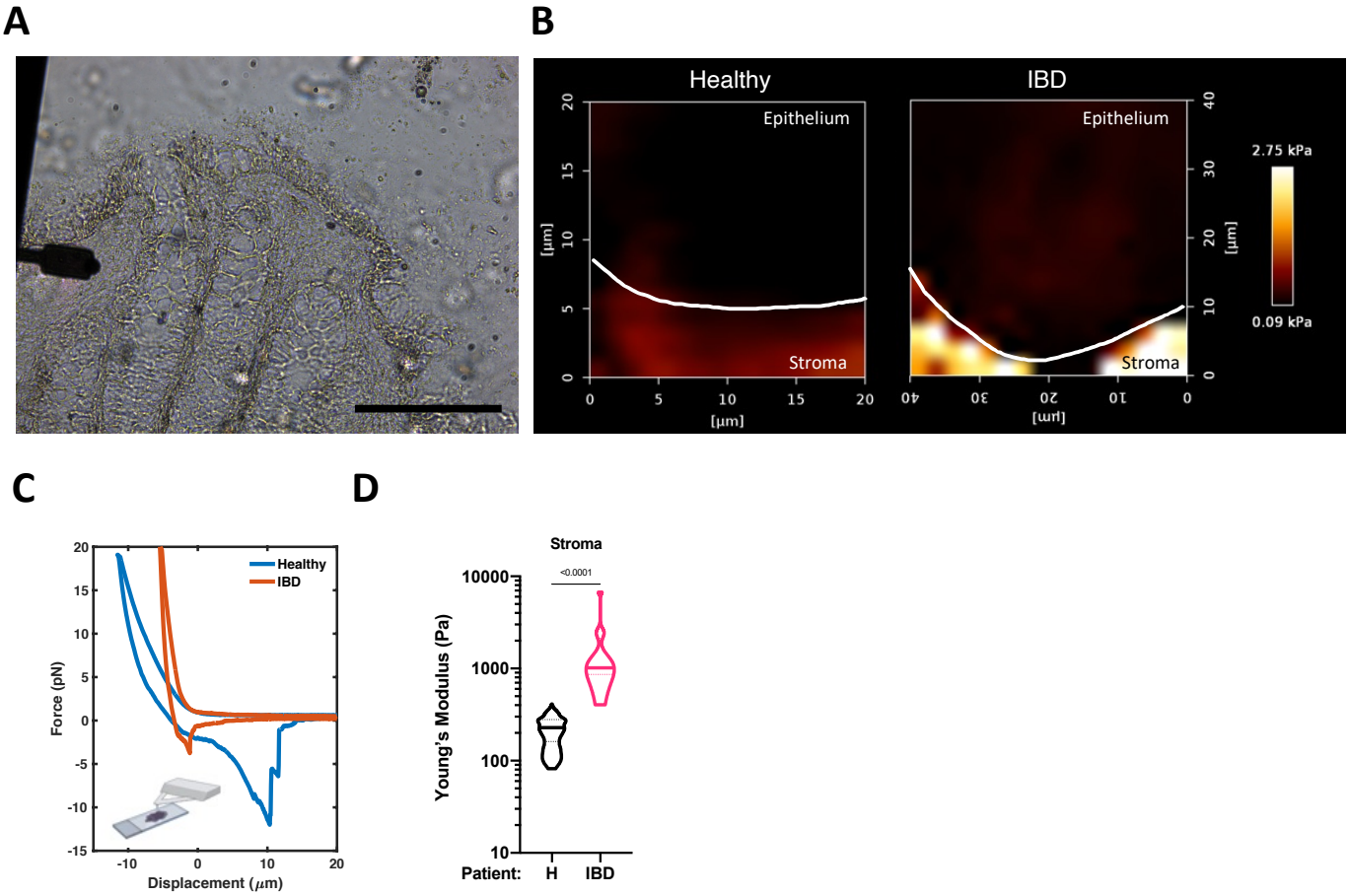

Extended Data Fig. 5

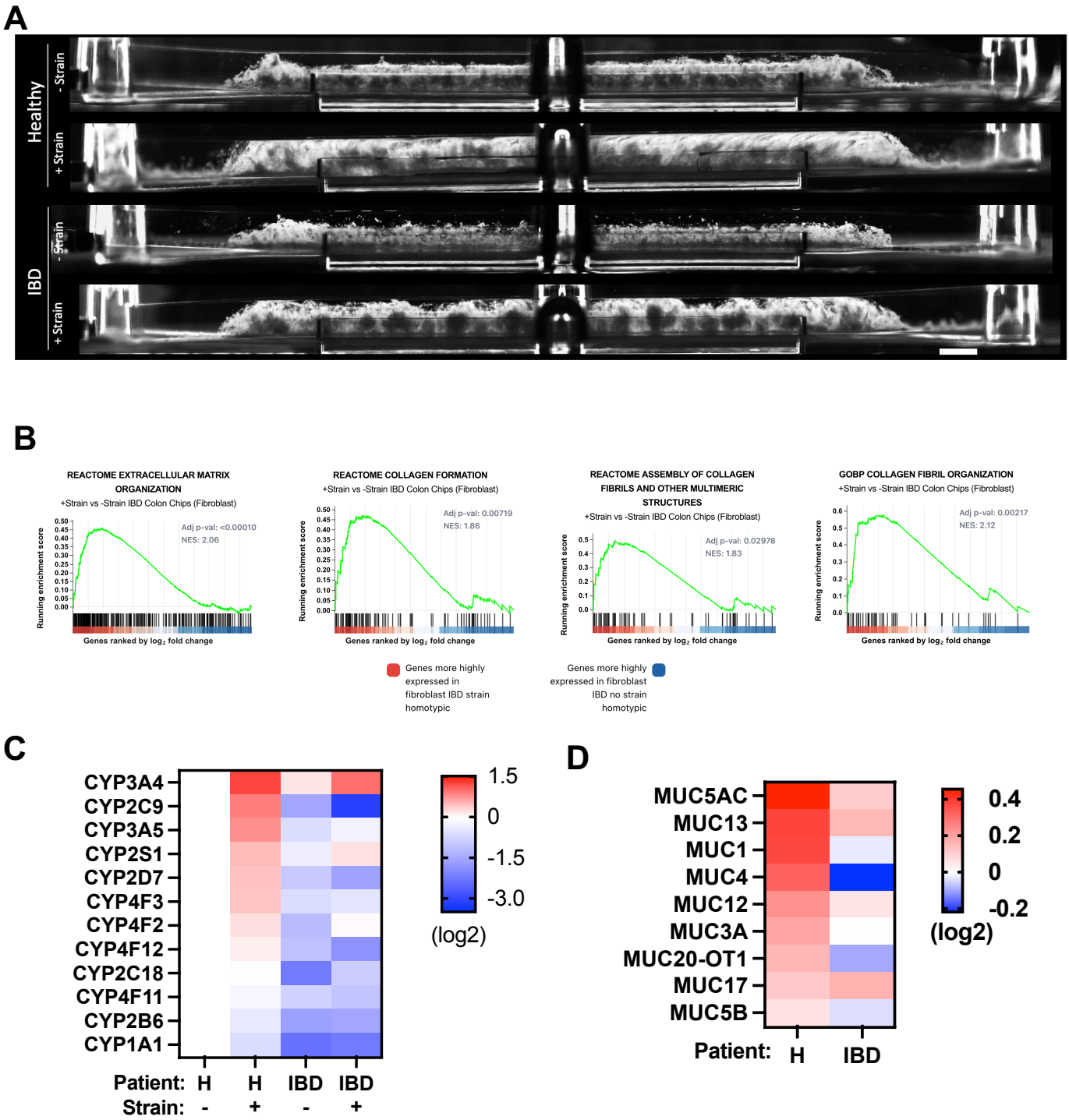

Extended Data Fig. 6

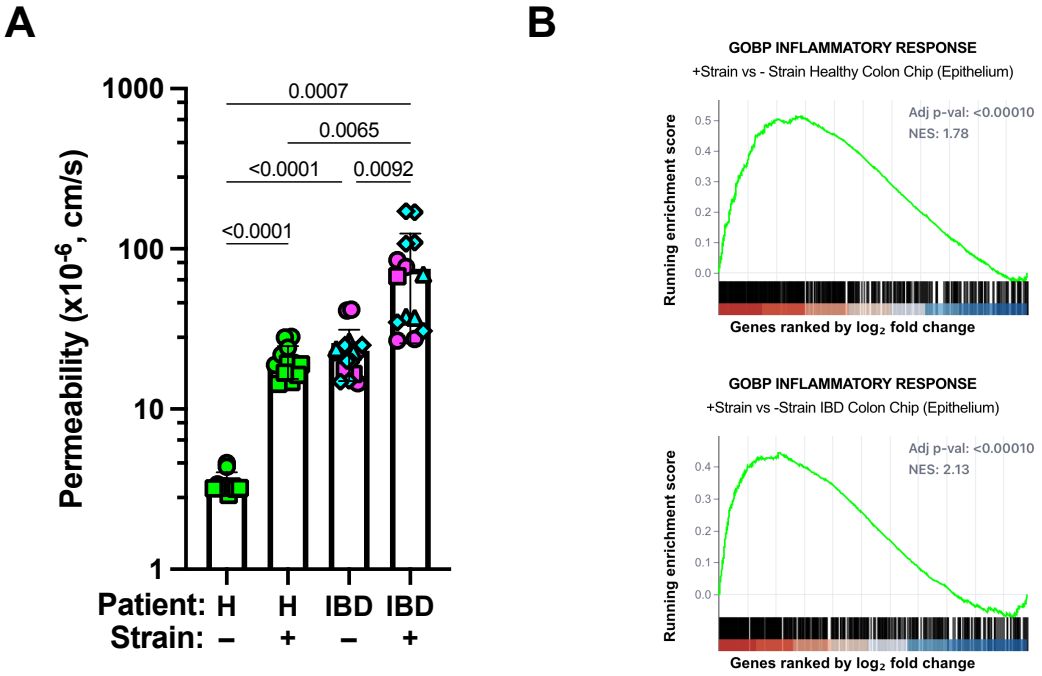

Extended Data Fig. 7

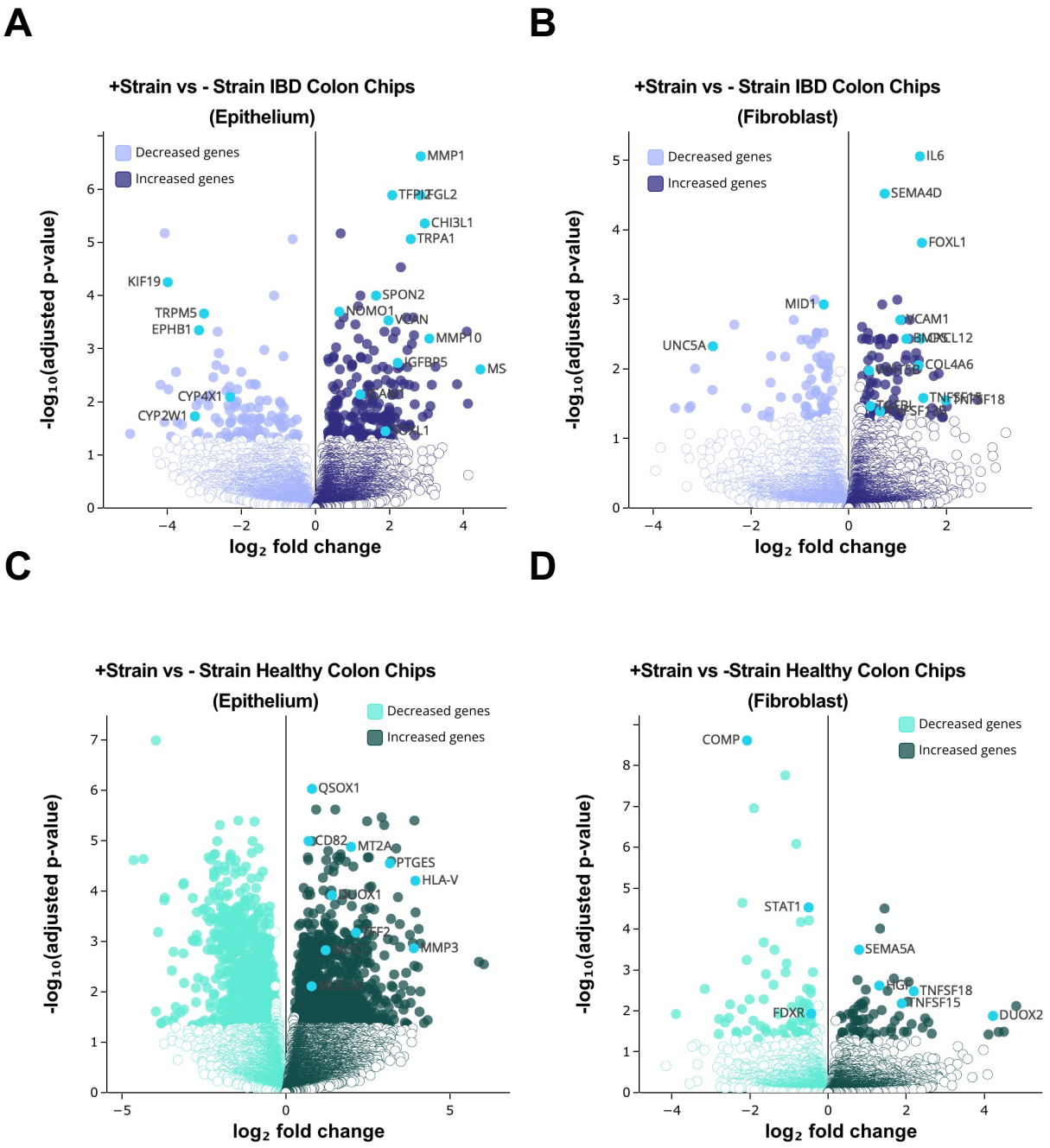

Extended Data Fig. 8

A

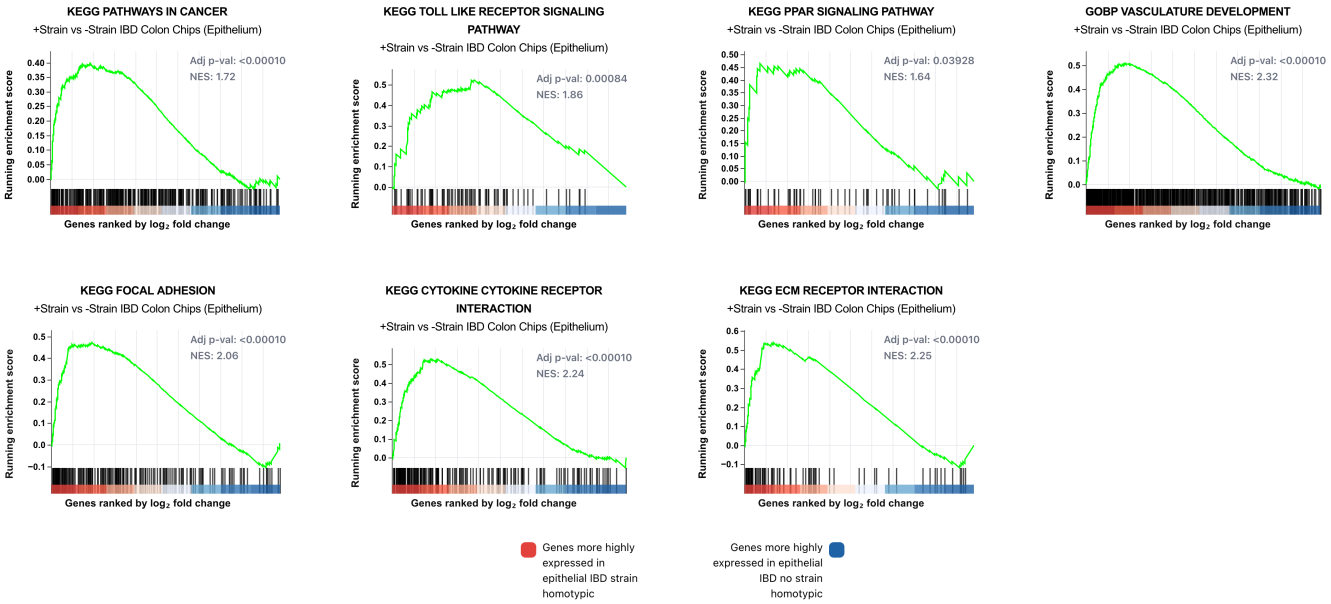

B

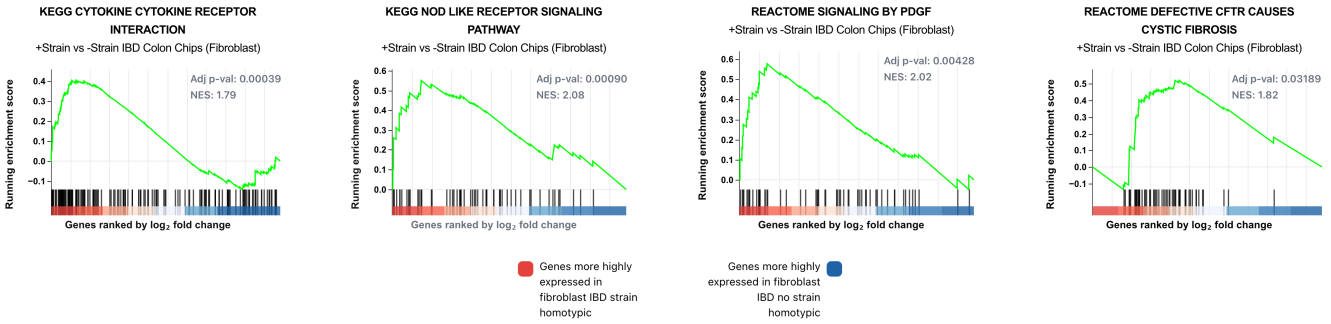

Extended Data Fig. 9

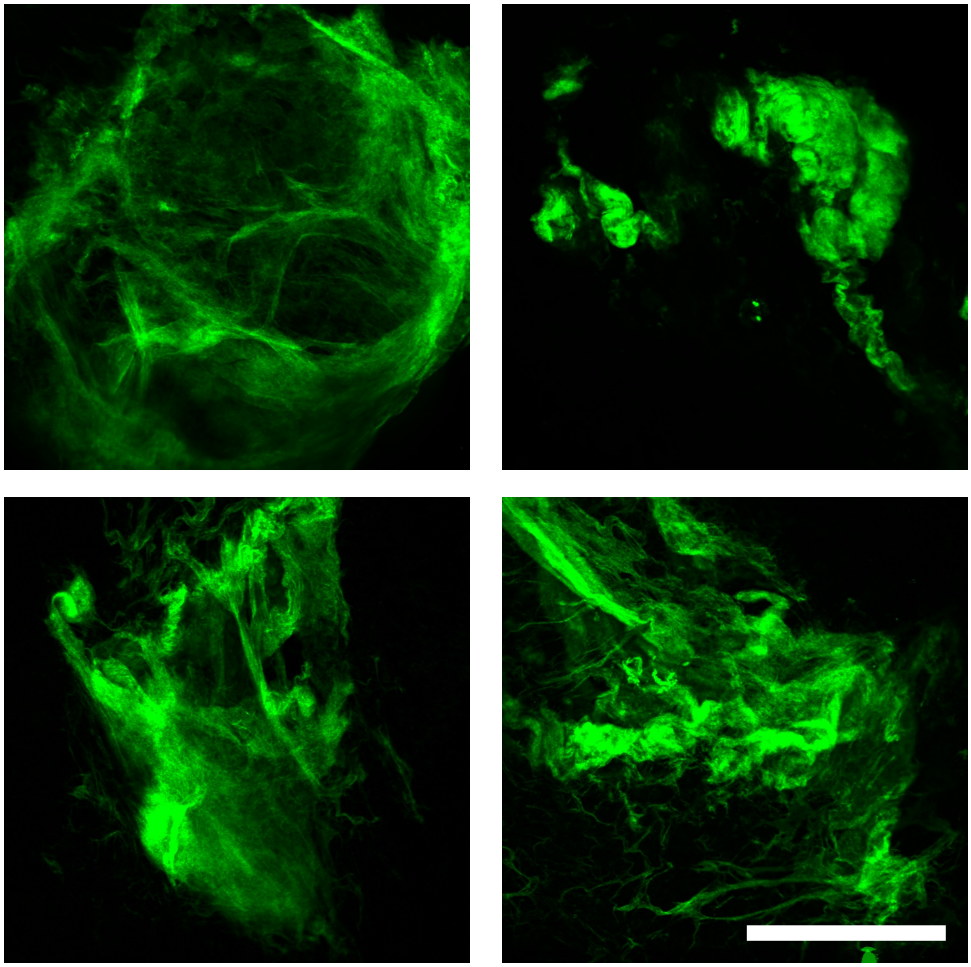

Extended Data Fig. 10

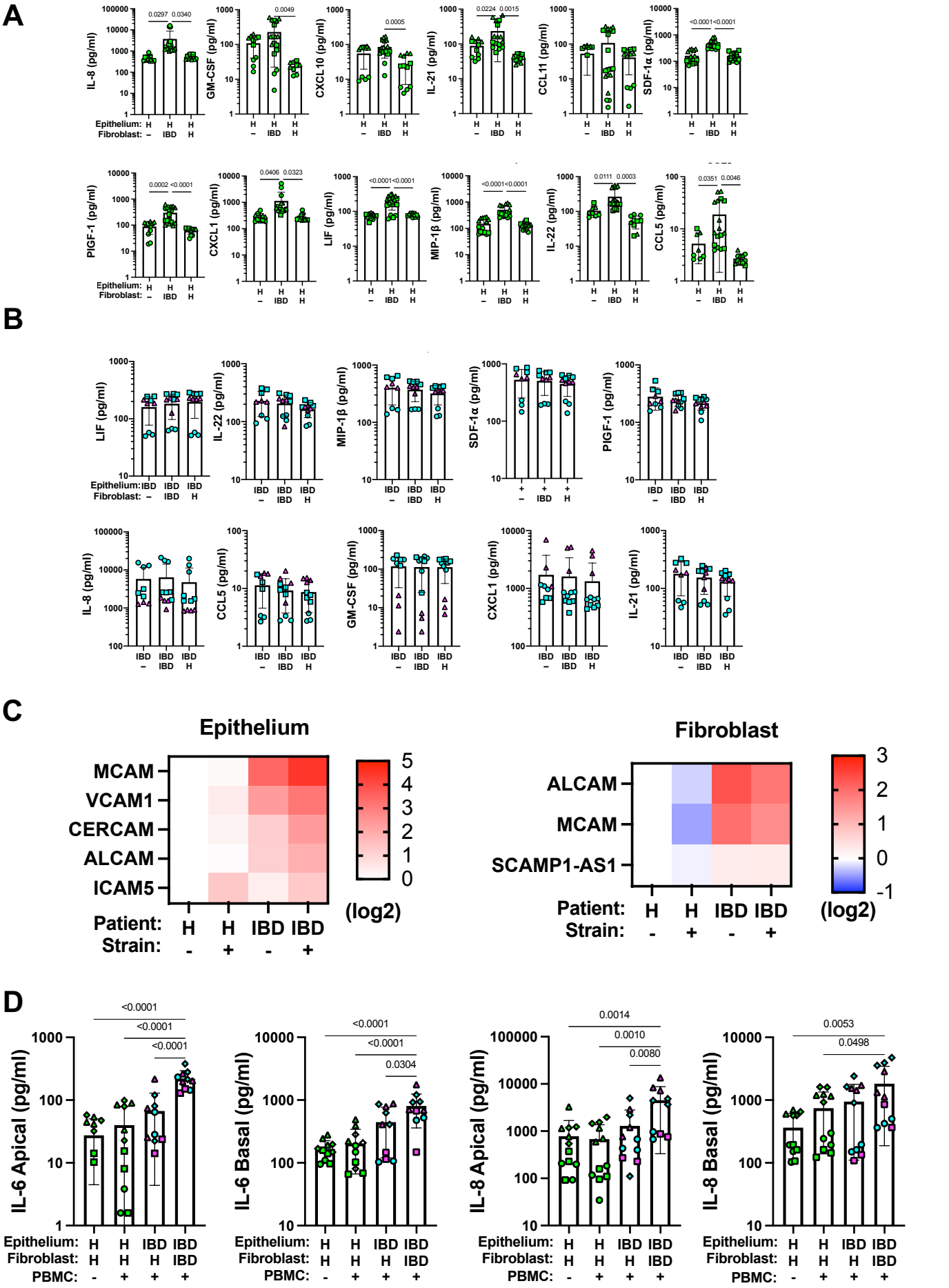

Extended Data Fig. 11

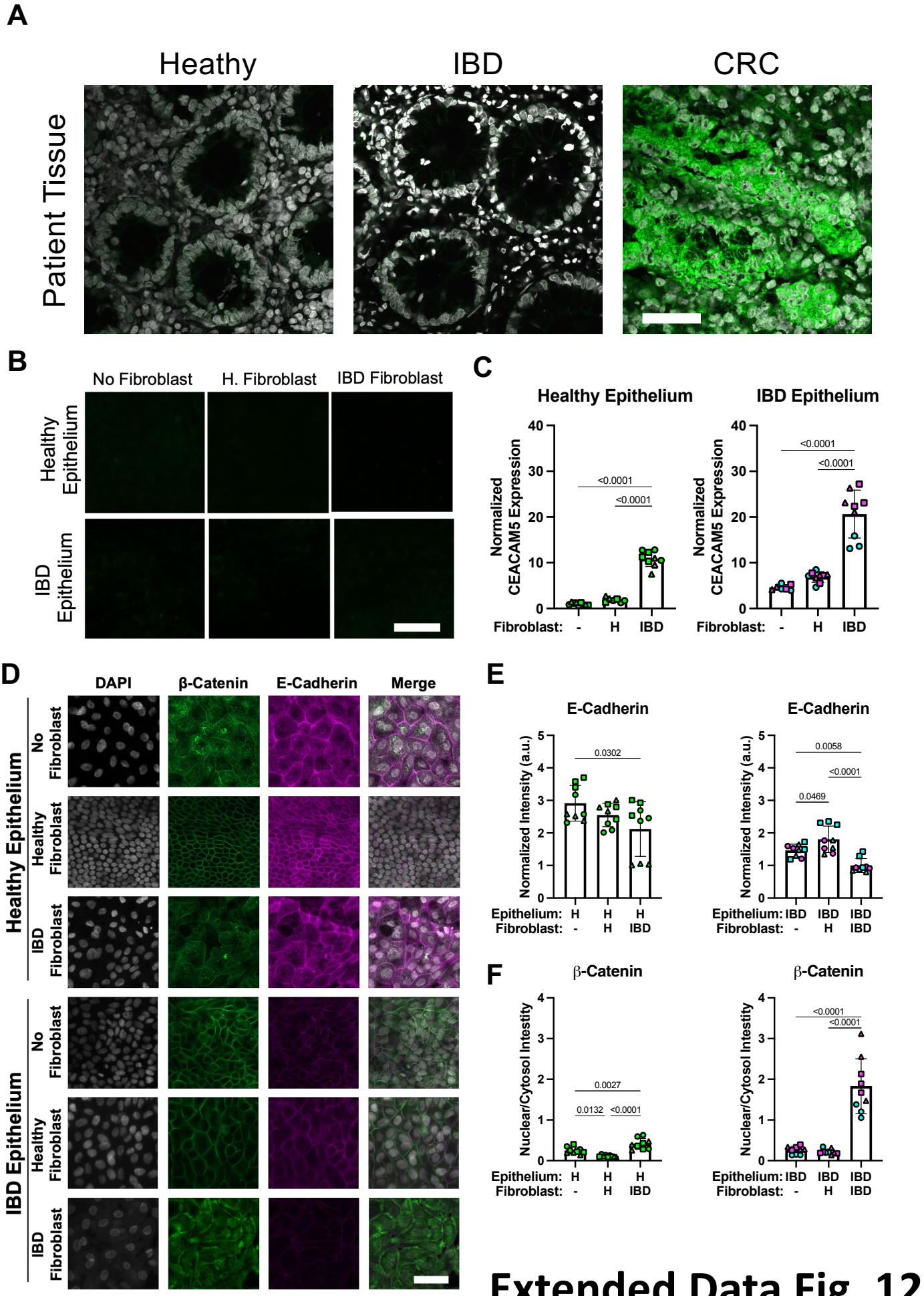

Extended Data Fig. 12

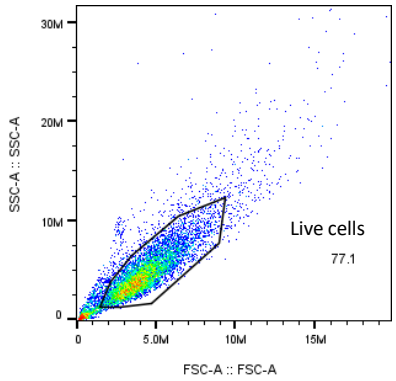

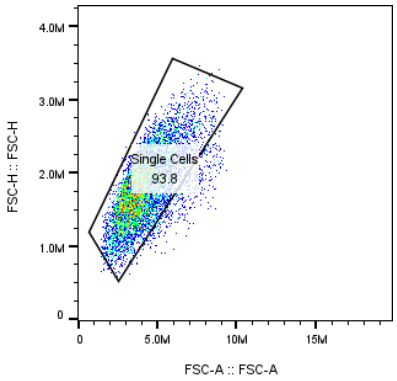

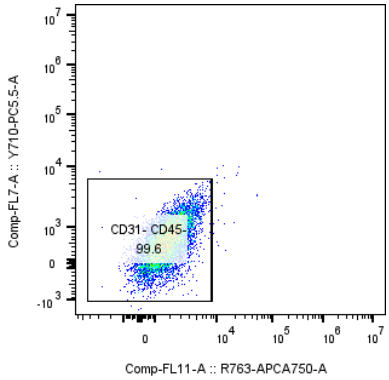

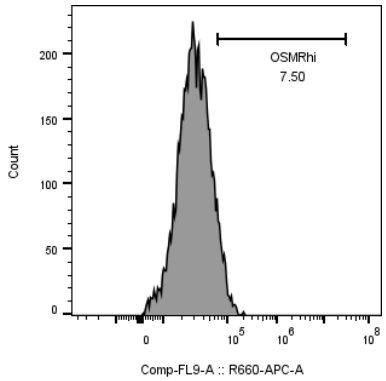

Supporting Data Fig. 1